12-2016

An investigation of composite failure analyses and damage evolution in finite element models

Ann M. Frappier
Purdue University

Graduate School Form
30 Updated 12/26/2015

PURDUE UNIVERSITY
GRADUATE SCHOOL
Thesis/Dissertation Acceptance

This is to certify that the thesis/dissertation prepared

By Ann M. Frappier

Entitled

AN INVESTIGATION OF COMPOSITE FAILURE ANALYSES AND DAMAGE EVOLUTION IN FINITE ELEMENT MODELS

For the degree of Master of Science in Engineering

Is approved by the final examining committee:

Vikas Tomar
Chair

Thomas S. Siegmund

Wenbin Yu

To the best of my knowledge and as understood by the student in the Thesis/Dissertation Agreement, Publication Delay, and Certification Disclaimer (Graduate School Form 32), this thesis/dissertation adheres to the provisions of Purdue University's "Policy of Integrity in Research" and the use of copyright material.

Approved by Major Professor(s): Vikas Tomar

Approved by: Dale A. Harris 12/2/2016

Head of the Departmental Graduate Program Date

AN INVESTIGATION OF COMPOSITE FAILURE ANALYSES AND DAMAGE EVOLUTION IN FINITE ELEMENT MODELS

A Thesis

Submitted to the Faculty

of

Purdue University

by

Ann M. Frappier

In Partial Fulfillment of the

Requirements for the Degree

of

Master of Science in Engineering

December 2016

Purdue University

West Lafayette, Indiana

For my Mother, soon-to-be Husband, Miss Maggie, and Miss April

ACKNOWLEDGEMENTS

I would like to express my deepest gratitude for the constant support and guidance of the following individuals who each, in their own way, have contributed to this feat.

To Dr. Vikas Tomar, for his guidance, availability, and support which helped in the successful completion of my work.

To Mr. Christopher Jared Cone for his abundant love and belief in myself that propelled my efforts.

Finally, to my mother, Ms. Mary Ann Bugea Frappier who without her sacrifices, commitment to my education, and continuous prayers would not have compelled me to achieve. You will always be a source of strength for me.

TABLE OF CONTENTS

Page

Page

LIST OF TABLES

LIST OF FIGURES

Figure Page

ABSTRACT

Frappier, Ann M. M.S.E., Purdue University, December 2016. An Investigation of Composite Failure Analyses and Damage Evolution in Finite Element Models. Major Professor: Vikas Tomar.

This paper presents a composite conical structure used commonly in flight-qualification testing. This structure's overall load-displacement behavioral response is characterized. Mixed-mode multidelamination in a layered composite specimen is considered in Abaqus/Explicit through both the Virtual Crack Closure Technique and Cohesive Elements. The Virtual Crack Closure Technique and Cohesive Elements are compared against experimental test results presented in literature. Further, a thorough comparison in which the effects of failure criteria type, through-thickness mesh density, and finite element type on the progressive failure response of this composite assembly is discussed. Lastly, Abaqus/Standard and Helius PFA are compared in order to gain confidence into which analytical model's failure theories best predicts the different scales of failure, both local/microscale and global/macroscale.

CHAPTER 1. INTRODUCTION

1.1 Background

In 1991 the UK Science and Engineering Research council (known today as the Engineering and Physical Sciences Research Council) and the UK Institution of Mechanical Engineers (I Mech E) met concerning the subject of "Failure of Polymeric Composites and Structures: Mechanisms and Criteria for the Prediction of Performance [7]." The outcomes and continuing work from which are compiled in *Failure Criteria in Fibre Reinforced Polymer Composites: The World-Wide Failure Exercise* [7]. The meeting aimed to establish confidence in academia and industry in the present methodology for failure prediction of Fiber Reinforced Composites. This meeting demonstrated two key findings [7]:

1. Skepticism in the present failure criteria in use

   At the lamina or even the laminate level, attendees determined evidence was insufficient to demonstrate which criteria, if any, could produce meaningful and accurate failure predictions.

2. No universal definition of a composite 'failure'

   In brevity, a designer would state that 'failure' is the moment at which the structure stops fulfilling its function. This definition of failure is use specific. As such, attendees determined that this definition did not establish the

needed link between events at the lamina level and the many invoked definitions of structural failure. Therefore, at the meeting's conclusion, this link remained to be established.

These findings might be surprising to some considering that for the past fifty years there has been a large amount of research into composite materials as primary load bearing structures. Everyday items such as airplanes, boat hulls, etc use composite materials [7]. However, failure theories are often used to initially 'size' a component while after such a 'sizing' they are disregarded in accurately predicting the ultimate strength of the structure. Furthermore, beyond this 'sizing', experimental tests on coupons or structural elements are often used to determine the global design allowables. The aerospace industry widely uses this approach to establish large databases of composite materials' allowables, such as the Advanced General Aviation Technology Experiements (AGATE) database, at great expense. This 'make and test' approach and use of generous safety factors is common; however, in niche markets confidence has built up in failure theory predictions and is leading to reduced margins [7].

In the recent past minimal motivation has been invested into the need for researching and developing improved failure theories. Some have adopted the perspective that failure theories are more of an academic curiosity than a practical design aid. This belief for the most part has begun to alter. The need for the use of failure theories in design has increased due to the demand to reduce the time and cost associated with bringing new components to the market. Similarly, the 'make and test' approach is widely reducing in number due to time and cost constraints. There is a need to improve design methods. This cannot be accomplished without the use of analytical modeling [7].

Analytical models for fiber composite structures have been widely available for more than fifteen years [7]. There are numerous analytical software products available. These range from small software codes, which represent laminate plate theory, to large software codes that have the capability to simulate the structural response of an entire composite assembly. For the most part, these software packages consist of one or more failure theories which the developer has chosen to implement from literature. The selected failure theories' implementation into a software code can influence the code's failure predications. Therefore, there is no guarantee that a Finite Element (FE) idealization of a theory in an analytical model will produce identical results [7]. Thus, it is of particular interest to study the ability of a FE code to capture the failure response behavior of a composite structure [7].

1.2 Motivation

The last fifteen years has seen an overwhelming amount of activity in the subject of composites research. This activity has predominantly been in the development of composite progressive damage analysis methods (PDA) [27]. During the year 2014-2015 the Air Force Research Laboratory (AFRL) conducted a program entitled "Damage Tolerance Design Principles (DTDP)" to evaluate the existing technology in composite damage progression modeling and prediction [27]. AFRL's research on this topic is motivation for this current study in which it is of interest to evaluate existing analytical tools in order to compare and find confidence in them to support present damage growth analysis needs.

In FE Modeling the progressive failure response of a composite structure is affected by failure criteria type, through-thickness mesh density, and finite element type.

In most composite structures, catastrophic macroscale failure is prompted by the onset and growth of microscale or localized matrix and fiber constituent failures. Two scales of failure are the motivators for this research [1]:

1. Microscale Failure (local failure at a Gaussian integration point):
    a. Matrix Constituent Failure
    b. Fiber Constituent Failure
2. Macroscale Failure (Catastrophic Failure, discrete reduction in global stiffness of the structure)

1.3 Overview

The Air Force Research Laboratory Space Vehicles Directorate (AFRL/RV) directed CSA Engineering to perform structural failure testing on key large aerospace composite structures, specifically one of which was a composite conical assembly (Figure 1.1 [3]).

Figure 1.1 AFRL/CSA Composite Adapter Failure Test Articles [3]

This type of quasi-static monotonically increasing load testing is critical in determining applied flight and qualification load levels and is typically conducted until structural failure is achieved. Further, this type of test is typically driven by data attained through composite coupon tests, which are uninspired by analytical techniques. Additionally, the

design of these tests is often encompassed by company specific knock-down factors. These knock-down factors inevitably contain a host of potential issues, real or assumed. Therefore, through instrumentation and video cameras used in testing events, data is collected to determine failure initialization and propagation to correlate with analytical predictions of structural response and ultimate failure. In this manner it can be ascertained if the composite structure's design is overly conservative or appropriate for the intended application [3].

AFRL's research on damage progression modeling and prediction [27], AFRL/CSA's composite assembly [3], its corresponding structural flight-qualification loading event [3], and noticeable lack of confidence in the use of analytical models to predict failure and reliance on accompanying testing of structures, as noted in key finding number one of the *World-Wide Failure Exercise (WWFE)* [7], are the inspiration for this research. Therefore, it is of interest to model a design of a composite assembly (similar to that shown in Figure 1.1) that would be used in this type of flight-qualification event. Further, it is desired to study the ability of Abaqus/Explicit to predict mixed-mode multidelamination in a layered composite specimen. This study will be accomplished via the Virtual Crack Closure Technique (VCCT) and via Cohesive Elements (CE). This information will prove pertinent should a delamination-type event arise during flight-qualification testing. Additionally, an exploration in the ability of FE Modeling to predict failure via matrix constituent failure, fiber constituent failure, and global failure observing the effects of: linear elastic analysis, first failure analysis, through-thickness mesh density, and element type is of curiosity. Lastly, various failure theories: Maximum Stress, Tsai-Wu, Multicontinuum Theory, and Hashin will be compared in order to build

confidence into which failure theory is best suited to predict the behavioral response of this composite structure.

1.4 Objective

A group of quasi-static monotonically increasing loads on a composite structure is imposed. From this it is possible to capture the structure's overall response characterized by the displacement of certain points on the structure. Catastrophic failure is found by a noticeable discontinuity in the structure's load-displacement curve indicative of a significant decrease in the total stiffness of the structure. The objective of such an investigation is to:

1. Determine Abaqus/Explicit's ability to predict mixed-mode multidelamination in a layered composite specimen through the employment of the VCCT and CE.
2. Determine the effects of failure criteria type, through-thickness mesh density, and finite element type on the progressive failure response of the composite assembly.
3. Use software applications Abaqus/Standard and Helius PFA to understand the different types of failure (local, microscale and global, macroscale) predictions and compare their results.

1.5 Scope

The conic part is modeled as a sandwich construction (See Chapter 5, Section 1). The loads are simulated based on flight-qualification testing using four actuators (See Chapter 5, Section 4). Further, the loads are quasi-static and are linearly ramped.

A side-study will be performed to assess the ability of Abaqus/Explicit in predicting a mixed-mode multidelamination event in a layered composite specimen via:

1. Virtual Crack Closure Technique (VCCT)

2. Cohesive Elements (CE)

To analyze the effect of failure criteria type, through-thickness mesh density, and finite element type on the progressive failure of this conical composite the following analyses will be performed:

1. Linear Elastic Analysis
2. First Failure Analysis
3. Effect of Through-Thickness Mesh Density
4. Effect of Element Type

Additionally, different scales of failure theories will be assessed and their results compared. This composite structure will be analyzed with the following linear elastic, microscale (local) failure theories:

1. Max Stress
2. Tsai-Wu
3. Multicontinuum Theory (MCT)

Macroscale (Catastrophic) progressive damage model theories will also be considered and their results compared. The composite structure will be analyzed with the following:

4. Hashin
5. Multicontinuum Theory (MCT)

Finally, the conclusion of the above efforts will showcase a thorough comparison of linear elastic failure theories with progressive damage models in an effort to understand the capabilities of analytical modeling. The scope of the above efforts is presented below in Figure 1.2.

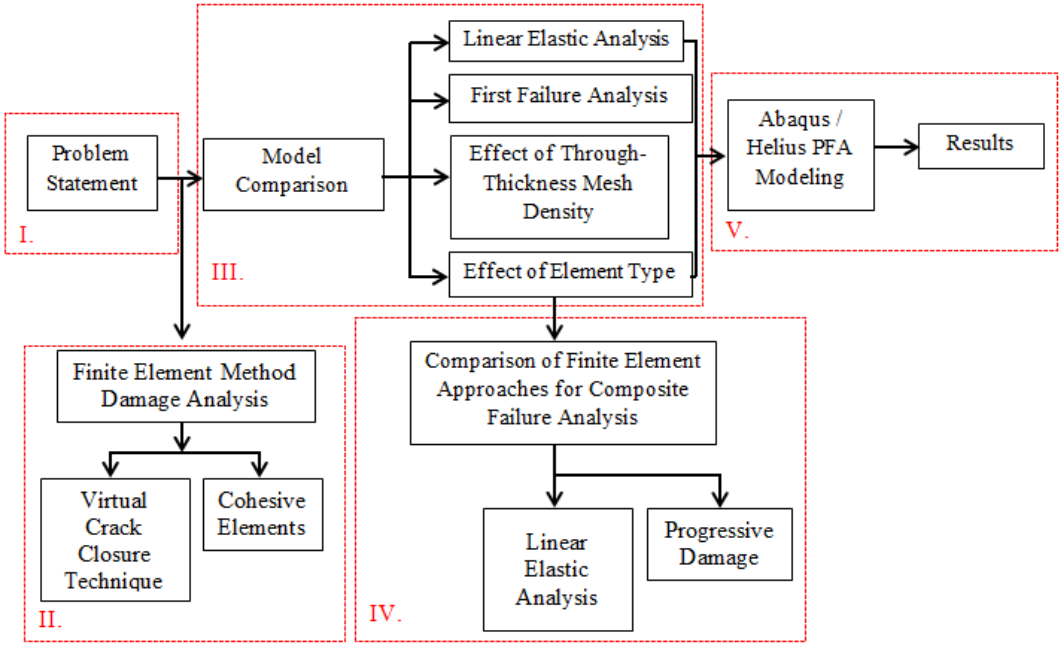

Figure 1.2 Scope of Project

CHAPTER 2. FINITE ELEMENT METHODS DAMAGE ANALYSIS

2.1 Delamination in Composite Structures

Modern aircraft structures are trending towards the substitution of composite over metallic materials. This is for the reason that composites exhibit superior structural properties: increased permissible stress, increased fatigue and damage tolerance, decreased sensitivity to corrosion, etc. [2].

These compelling reasons to use composites; however, do have a drawback when compared with metallic materials. Composites can delaminate. In fact, this failure mode is typical. Inter-laminar delamination, more commonly called delamination, is a loss of cohesion between adjacent plies in a laminate. The origination of delamination is most often caused by design features prone to develop inter-laminar stresses. Examples of these could be: curved sections, drop-offs, free edges, among others. However, origination can also be from manufacturing defects, such as: matrix shrinkage during cure, formation of resin-rich areas, etc. Even still accidents such as tool impacts can cause delamination. Cyclic loading behavior can cause debonding (interfacial failure) and microscale damage to the matrix, which ultimately induces delamination. Hence, inter-laminar delamination can be caused by a variety of reasons and as such should be carefully studied and understood in composite structures [2].

Part of understanding delamination in composite structures is to consider how it diminishes material properties which correspond to decreased load capacity. Furthermore,

a delamination tends to propagate under compression and out of plane loads. Presently, it is rule of thumb in the aircraft industry to use a strain design approach to cover impact damage and to avoid delamination growth. For monolithic laminates this limit is typically 3,500-4,000 με. Lower limits are often used for other laminates such as honeycomb panels [2].

In composites another area of concern for many aircraft structures is bonded joints. These tend to be stiffened panels, such as skin-ribs, skin-spar, etc. These joints are complicated to analyze for the reason that the stress distribution at the joints is complex typically showing high stress concentrations at its edges. The resulting progressive debonding is difficult to simulate [2].

Conservative designs are often the answer as was noted in the *WWFE* [7] due to the presumed shortage of accurate and dependable simulation methodologies. However, ample research has been performed in the recent past to develop suitable methods to simulate delamination type events [2]. It is in dealing with these complex composite structures and their corresponding damage (i.e. inter-laminar delamination) that FE techniques are often employed. VCCT and CE are two of the most common FE methods used to simulate delamination and debonding [4].

2.2 Virtual Crack Closure Technique (VCCT)

VCCT is derived from linear fracture mechanics and requires the calculation of the Strain Energy Release Rates (SERR) to predict delaminations or debonding growth. Pure modes of fracture (i.e. mode I, model II, and mode III) are the basis for calculating the SERRs. VCCT requires a pre-damaged structure. As such, damage onset is not able to be predicted with this theory [4, 11-13, 28].

In commercial FE software, such as Abaqus/Explicit, the SERR (G) is compared with fracture toughness (G_c) of the material being analyzed for either mode I, mode II, or mode III. Delamination is noticed when G exceeds or is equal to G_c as shown in Equation 2.1 [9].

$$G \geq G_c \tag{2.1}$$

Each mode has its own respective fracture mode. These fracture modes are each defined by the energy released. The energy released for each mode is the work done by the nodal forces needed to close the crack tip. As such, the fracture modes for mode I, mode II, and mode III are as follows in Equations 2.2-2.4 respectively [9]:

$$G_I = \frac{1}{2b\Delta a} F_{cd}^{y}(v_c - v_d) \tag{2.2}$$

$$G_{II} = \frac{1}{2b\Delta a} F_{cd}^{x}(u_c - u_d) \tag{2.3}$$

$$G_{III} = \frac{1}{2b\Delta a} F_{cd}^{yz}(w_c - w_d) \tag{2.4}$$

Where:

b = specimen thickness

F = magnitude of nodal forces pairs at nodes c and d in the y, x, and z direction

u = nodal displacement before nodes c and d are pulled together

v, u, and w = nodal displacement before nodes c and d are pulled together

Figure 2.1 [9] below is a visual representation of the calculation of the energy release rate using VCCT.

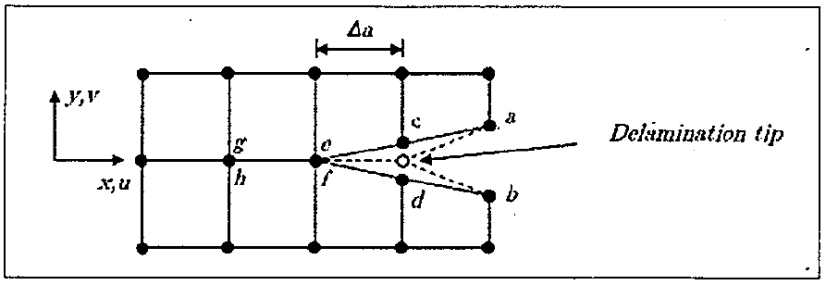

Figure 2.1 Energy Release Rate Calculation using VCCT [9]

Once G_I, G_{II}, G_{III}, have been determined, the total energy release rate can be calculated as seen in Equation 2.5 [9]:

$$G_T = G_I + G_{II} + G_{III} \tag{2.5}$$

Afterwards, as previously provided, delamination can be found if the condition in Equation 2.1 is found to be true [9].

2.3 Cohesive Elements

CE, known commonly as the Cohesive Zone Model (CZM), is derived from damage mechanics [4, 26, 30] and considered to originate from the works of Hilleborg [25]. In contrast to VCCT it does not require a pre-damaged structure to predict delamination and debonding growth. This allows for damage onset to be determined [4].

This study focuses on the commercial FE software Abaqus/Explicit. In Abaqus/Explicit cohesive elements capture relations that provide a description of the evolution of tractions (T) generated across the faces of a crack as a function of the crack face displacement jump (Δ). The implementation of cohesive elements requires the use of additional bulk finite elements. These elements are necessary to model [9, 14-24]:

1. Stage surrounded by cohesive surface elements (see Figure 2.2 and Figure 2.3 below [9])
2. Crack initiation

3. Crack evolution
4. Complete failure

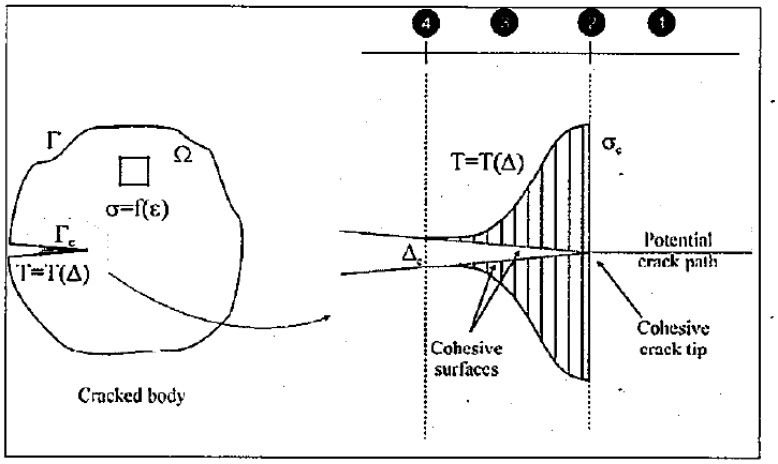

Figure 2.2 CZM of Fracture [9]

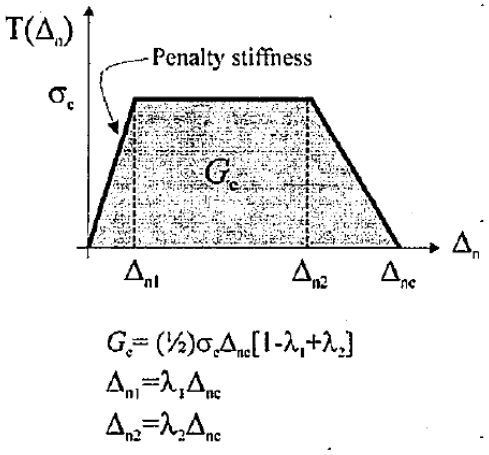

Where the Governing Cohesive Parameters are:
G_c= Cohesive Fracture Energy
σ_c= Peak Stress (Cohesive Strength of Material)
Δ_{nc}= Critical Opening Displacement
λ_1 and λ_2 are values that dictate the shape of $T = T(\Delta_n)$

Figure 2.3 Cohesive Law [9]

Equation 2.6 represents the contribution of the internal virtual work for bulk elements [9]:

$$G = \lim_{\Delta a \to 0} \frac{w}{\Delta a} \tag{2.6}$$

The contribution of the cohesive surface elements to the internal virtual work is given by Equation 2.7 [9]:

$$\int_{\Omega} \sigma : \varepsilon \, d\Omega - \int_{\Gamma_c} T\Delta_n \, d\Gamma_c - \int_{\Gamma} Pu \, d\Gamma = 0 \tag{2.7}$$

Where:

ε = virtual strain defined in the domain Ω associated to the virtual displacement u

Δ_n = virtual crack faces normal displacement jump along the crack line Γ_c

T = traction vector along the cohesive zone

P = external traction vector

Therefore, the FE formulation can be rewritten as Equation 2.8 [9]:

$$\left[\int_{\Omega} B^T E B \, d\Omega - \int_{\Gamma_c} N_c^T \, \frac{\partial T}{\partial \Delta_n} \, N_c d \, \Gamma_c\right] \, d = \, \int_{\Gamma} N^T P \, d\Gamma \tag{2.8}$$

Where:

N = matrix of shape functions for bulk elements

N_c= matrix of shape functions for cohesive elements

B = derivative of N

d = nodal displacements

E = tangential stiffness matrix for bulk elements

$\frac{\partial T}{\partial \Delta_n}$ = Jacobian stiffness matrix

Thus, in order to fully employ the use of this method the contribution of cohesive elements to the tangent stiffness matrix and force vector is acquired from the numerical implementation of the CE method [9].

CHAPTER 3. MATHEMATICAL FOUNDATIONS: FINITE ELEMENT APPROACHES FOR COMPOSITE FAILURE ANALYSIS

Composite failure theories have been a subject of concern for nearly fifty years. There are a variety of published theories to choose from when performing an analysis of a composite structure. However, none of these theories have successfully predicted the full range of observed behavior of a composite laminate [6]. Therefore, this section seeks to provide the mathematical background necessary to delve into the results presented in Chapter 7, Comparison of FE Approaches, using such criteria as: Maximum Stress, Tsai-Wu, Multicontinuum Theory (MCT), and Hashin in order to understand the assumptions and effects of the proposed theories in commercial FE codes.

3.1 Maximum Stress Failure Criterion

The Maximum Stress Criterion identifies composite material failure caused by three possible modes (longitudinal failure, transverse failure, and shear failure) of loading [1, 5].

Longitudinal failure occurs when [1, 5]:

$$\sigma_{11} \geq S_{11}^{+} \tag{3.1}$$

Or

$$\sigma_{11} \geq S_{11}^{-} \tag{3.2}$$

Transverse failure occurs when [1, 5]:

$$\sigma_{22} \geq S_{22}^{+} \tag{3.3}$$

Or

$$\sigma_{22} \geq S_{22}^{-} \tag{3.4}$$

Shear failure occurs when [1, 5]:

$$|\sigma_{12}| \geq |\sigma_{12}^{max}| \tag{3.5}$$

Where:

S_{11}^{+} = Maximum tensile strength in the fiber direction

S_{11}^{-} = Maximum compressive strength in the fiber direction

S_{22}^{+} = Maximum tensile strength transverse to the fiber direction

S_{22}^{-} = Maximum compressive strength transverse to the fiber direction

σ_{12} = Maximum in-plane shear stress

3.2 Tsai-Wu Failure Criterion

Unlike the Maximum Stress Criterion the Tsai-Wu Criterion does not distinguish between different modes of failure. Instead it is a quadratic, interactive stress-based criterion that identifies failure.

Failure occurs when [1]:

$$F_1\sigma_{11} + F_2\sigma_{22} + F_{11}\sigma_{11}^2 + F_{22}\sigma_{22}^2 + F_{66}\sigma_{12}^2 + 2F_{12}\sigma_{11}\sigma_{22} \geq 1 \tag{3.6}$$

Where:

$$F_1 \equiv \frac{1}{S_{11}^{+}} - \frac{1}{S_{11}^{-}} \tag{3.7}$$

$$F_2 \equiv \frac{1}{S_{22}^{+}} - \frac{1}{S_{22}^{-}} \tag{3.8}$$

$$F_{11} \equiv \frac{1}{S_{11}^{+}S_{11}^{-}} \tag{3.9}$$

$$F_{22} \equiv \frac{1}{S_{22}^{+}S_{22}^{-}} \tag{3.10}$$

$$F_{66} \equiv \frac{1}{S_{12}S_{12}} \tag{3.11}$$

The interaction term F_{12} is defined as [1]:

For biaxial failure stress ($\sigma_{11} = \sigma_{22} = \sigma_{biaxial}$)

$$F_{12} \equiv \frac{1}{2\sigma_{biaxial}^2}\left[1 - \left(\frac{1}{S_{11}^+} + \frac{1}{S_{11}^+} + \frac{1}{S_{22}^+} + \frac{1}{S_{22}^+}\right)\sigma_{biaxial} + \left(\frac{1}{S_{11}^+ S_{11}^+} + \frac{1}{S_{22}^+ S_{22}^+}\right)\sigma_{biaxial}^2\right] \quad (3.12)$$

Otherwise [1]

$$F_{12} \equiv f^* \sqrt{F_{11} F_{22}} \quad (3.13)$$

Where:

$-0.5 \leq f^* \leq 0$

$S_{11}^+ = \sigma_{11}$ at longitudinal tensile failure

$S_{11}^- = \sigma_{11}$ at longitudinal compressive failure

$S_{22}^+ = \sigma_{22}$ at transverse tensile failure

$S_{22}^- = \sigma_{22}$ at transverse compressive failure

$S_{12} = |\sigma_{12}|$ at longitudinal shear failure

3.3 Multicontinuum Theory (MCT) Failure Criterion

The basis of a multicontinuum is to reflect the distinctly different materials that coexist within a Representative Volume Element (RVE). A unidirectional fiber composite material can be viewed as two interacting continua (a fiber continuum and a matrix continuum) that coexist in a RVE. In such a RVE there are three different volume averages relevant to the mechanics of the composite material. They are as follows [1]:

1. Physical quantities of interest are averaged over the whole RVE that represents the composite material. Traditionally, these quantities are 'homogenized' composite quantities and represent the overall averages of the physical quantities

as they vary over the fiber and matrix constituents of the microstructure within the RVE.

2. Physical quantities of interest are averaged specifically over the fiber continuum within the RVE of the composite material. These are fiber average quantities.
3. Physical quantities of interest are averaged specifically over the matrix continuum within the RVE of the composite material. These quantities are matrix average quantities.

Multicontinuum Theory augments traditional continuum mechanics by adding [1]:

1. The development of connections between various constituent average quantities of interest.
2. The development of connections that associate composite average quantities to constituent average quantities.

Fiber reinforced composite materials contain substantial differences in the strengths of their individual constituent materials. Based upon this fact a widely accepted approach is formulating failure criteria for the constituent materials (i.e. the fiber and matrix). However, limited success has been reached in basing constituent failure criteria on the composite average stress state. This is due to the fact that the composite average stress state is not solely relevant to the fiber or matrix constituent materials. Instead the composite average stress state represents the stress that would be present in a fictitious, statically equivalent, smeared material. In this regard, what should be done is base the constituent failure criteria on the constituent average stress state. This approach is what the software program Helius PFA uses. Explicitly stated, Helius PFA uses separate

failure criteria for each constituent material and bases the constituent failure criteria on the constituent average stress state [1].

3.3.1 Matrix Constituent Failure Criterion for Unidirectional Composites

In developing the Matrix Constituent Failure Criterion there exist the following assumptions [1]:

1. Matrix failure is assumed to be influenced by all six of the matrix average stress components σ_{11}^{m}, σ_{22}^{m}, σ_{33}^{m}, σ_{12}^{m}, σ_{13}^{m}, and σ_{23}^{m}.
2. The matrix constituent material is assumed to be transversely isotropic. The contributions of σ_{22}^{m} and σ_{33}^{m} or σ_{12}^{m} and σ_{13}^{m} to matrix failure are not distinguishable.
3. The influence of the matrix average normal stresses (σ_{11}^{m}, σ_{22}^{m}, and σ_{33}^{m}) in producing matrix failure depends upon whether the normal stresses are tensile or compressive.
4. The matrix constituent is assumed to be transversely isotropic; however, matrix failure is assumed to be an isotropic event. When matrix failure occurs, each of the matrix average moduli (E_{11}^{m}, E_{22}^{m}, E_{33}^{m}, G_{12}^{m}, G_{13}^{m}, G_{23}^{m}) are reduced to a user-defined percentage of their original values, while the matrix average Poisson ratios (ν_{12}^{m}, ν_{13}^{m}, ν_{23}^{m}) are assumed to remain unchanged. Note: This stiffness reduction scheme infers that there is only one matrix failure mode regardless of the stress components that cause matrix failure and it results in a uniform degradation of matrix stiffness.

The Matrix Failure Criterion is then [1]:

$$\pm A_1^m (I_1^m)^2 - \pm A_2^m (I_2^m)^2 + A_3^m I_3^m + A_4^m I_4^m - \pm A_5^m I_1^m I_2^m = 1 \qquad (3.14)$$

Where:

$I_i^m (i = 1, 2, 3, 4)$ are transversely isotropic invariants of the matrix average stress state.

$$I_1^m \equiv \sigma_{11}^m \tag{3.15}$$

$$I_2^m \equiv \sigma_{22}^m + \sigma_{33}^m \tag{3.16}$$

$$I_3^m \equiv (\sigma_{22}^m)^2 + (\sigma_{33}^m)^2 + 2(\sigma_{23}^m)^2 \tag{3.17}$$

$$I_4^m \equiv (\sigma_{12}^m)^2 + (\sigma_{13}^m)^2 \tag{3.18}$$

$A_j^m (j = 1,2,3,4,5)$ are adjustable coefficients of the matrix failure criteria

Note: The Matrix Failure Criterion contains ten adjustable coefficients (I_i^m and $\pm A_j^m$) that must be determined using measure strengths of the composite material [1].

3.3.2 Fiber Constituent Failure Criterion for Unidirectional Composites

In developing the Fiber Constituent Failure Criterion there exist the following assumptions [1]:

1. Fiber failure is assumed to be influenced by the fiber average stress components σ_{11}^f, σ_{12}^f, and σ_{13}^f.
2. Fiber failure is assumed to be independent of the fiber average stress components σ_{22}^f, σ_{33}^f, and σ_{23}^f.
3. The contribution of σ_{11}^f in producing fiber failure depends upon whether σ_{11}^f is tensile or compressive.
4. The fiber constituent is assumed to be transversely isotropic. The contributions of σ_{12}^f and σ_{13}^f to fiber failure are not distinguishable.
5. The fiber constituent is considered to be a transversely isotropic material; however, fiber failure is assumed to be an isotropic event. When fiber failure occurs, each of the fiber average moduli (E_{11}^f, E_{22}^f, E_{33}^f, G_{12}^f, G_{13}^f, G_{23}^f) are

reduced to a user-defined percentage of their original values, while the fiber average Poisson ratios (ν_{12}^f, ν_{13}^f, ν_{23}^f) are assumed to remain unchanged.

Note: This stiffness reduction scheme infers that there is only one fiber failure mode regardless of the stress components that cause fiber failure and it results in a uniform degradation of all fiber moduli.

The Fiber Failure Criterion is then [1]:

$$\pm A_1^f \left(I_1^f\right)^2 + A_4^f I_4^f = 1 \tag{3.19}$$

Where:

$I_i^f\,(i = 1{,}4)$ are two transversely isotropic invariants of the fiber average stress state.

$$I_1^f \equiv \sigma_{11}^f \tag{3.20}$$

$$I_4^f \equiv \left(\sigma_{12}^f\right)^2 + \left(\sigma_{13}^f\right)^2 \tag{3.21}$$

$A_j^f\,(j = 1{,}4)$ are adjustable coefficients of the fiber failure criteria.

Note: The Fiber Failure Criterion contains three adjustable coefficients (I_i^f and $\pm A_j^f$) that must be determined using measure strengths of the composite material [1]. The fiber average stress components that make up the invariants are total stress terms (i.e. both mechanical and thermal stresses) [1].

3.3.3 Failure Criteria for Unidirectional Composites

The combination of the above Fiber Failure Criteria and Matrix Failure Criteria encompass the Failure Criteria for Unidirectional Composites. As such, thirteen constituent failure constituents are required using thirteen independent strength measurements. However, Helius PFA has adopted the approach that the strength data available for composite materials is in most cases limited to the following six industry-standard strength tests [1]:

1. $+S_{11}^{c}$ = longitudinal tensile strength (in the fiber direction)
2. $-S_{11}^{c}$ = longitudinal compressive strength (in the fiber direction)
3. $+S_{22}^{c} = +S_{33}^{c}$ = transverse tensile strength (transverse to the fiber direction)
4. $-S_{22}^{c} = -S_{33}^{c}$= transverse compressive strength (transverse to the fiber direction)
5. $S_{12}^{c} = S_{13}^{c}$ = longitudinal shear strength
6. S_{23}^{c} = transverse shear strength

Provided the above the makers of Helius PFA have developed highly successful empirical relationships using industry standard strength measurements to approximate composite strengths under various biaxial loads [1].

3.4 Hashin Failure Criterion

Four different modes of failure (tensile fiber failure, compressive fiber failure, tensile matrix failure, and compressive matrix failure) are identified by the Hashin Criterion [1, 10].

If $\sigma_{11} \geq 0$ then the Tensile Fiber Failure Criterion is [1, 10]:

$$\left(\frac{\sigma_{11}}{S_{11}^{+}}\right)^2 + \alpha\left(\frac{\sigma_{12}^2+\sigma_{13}^2}{S_{12}^2}\right) \geq 1 \tag{3.22}$$

Where:

α = contribution of the longitudinal shear stress to fiber tensile failure. The allowable range is $0 \leq \alpha \leq 1$. A default value for α is 0.

If $\sigma_{11} < 0$ then the Compressive Fiber Failure Criterion is [1, 10]:

$$\left(\frac{\sigma_{11}}{S_{11}^{-}}\right)^2 \geq 1 \tag{3.23}$$

If $\sigma_{22} + \sigma_{33} \geq 0$ then the Tensile Matrix Failure Criterion is [1, 10]:

$$\frac{(\sigma_{22}+\sigma_{33})^2}{S_{22}^{+\,2}} + \frac{\sigma_{23}^2-\sigma_{22}\sigma_{33}}{S_{23}^2} + \frac{\sigma_{12}^2+\sigma_{13}^2}{S_{12}^2} \geq 1 \tag{3.24}$$

If $\sigma_{22} + \sigma_{33} < 0$ then the Compressive Matrix Failure Criterion is [1, 10]:

$$\left[\left(\frac{S_{22}^-}{2S_{23}}\right)^2 - 1\right]\left(\frac{\sigma_{22}+\sigma_{33}}{S_{22}^-}\right) + \frac{(\sigma_{22}+\sigma_{33})^2}{4S_{23}^2} + \frac{\sigma_{23}^2-\sigma_{22}\sigma_{33}}{S_{23}^2} + \frac{\sigma_{12}^2+\sigma_{13}^2}{S_{12}^2} \geq 1 \tag{3.25}$$

Where for all the above:

$S_{11}^+ = \sigma_{11}$ at longitudinal tensile failure

$S_{11}^- = \sigma_{11}$ at longitudinal compressive failure

$S_{22}^+ = \sigma_{22}$ at transverse tensile failure

$S_{22}^- = \sigma_{22}$ at transverse compressive failure

$S_{12} = |\sigma_{12}|$ at longitudinal shear failure

$S_{23} = |\sigma_{23}|$ at transverse shear failure

CHAPTER 4. FINITE ELEMENT METHOD DAMAGE ANALYSIS MODELS

This study [4] illustrates the use of Abaqus/Explicit in the prediction of mixed-mode multidelamination in a layered composite specimen. Crack propagation analyses via the VCCT and via CE are employed.

4.1 Virtual Crack Closure Technique Model

4.1.1 Structural Description

The layered composite specimen (Figure 4.1 [8]) is 200 mm long with a total thickness of 3.18 mm and a width of 20 mm. The thickness direction is composed of twenty-four layers. The model has two initial cracks. The first crack has a length of 40 mm and is positioned at the mid-plane of the specimen at the left end. The second crack has a length of 20 mm and is located to the right of the first and two layers below. The model is composed of a top part consisting of twelve layers, a middle section consisting of two layers, and a bottom part consisting of ten layers. The FE Model can be seen in Figure 4.2. It is important to note that for the VCCT to be assigned in this model contact clearances must be defined, cohesive behavior properties must be specified, and crack propagation criteria with general contact must also be specified [4, 8, 29].

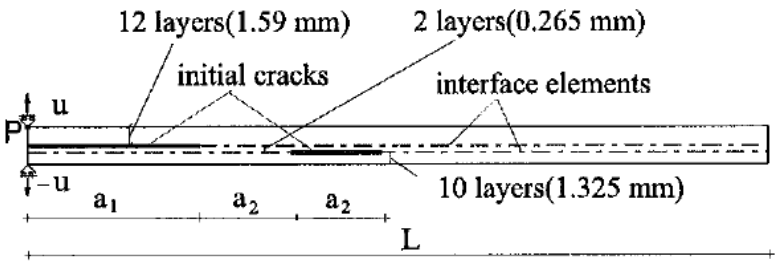

L=200 mm
a_1=40 mm
a_2=20 mm
width = 20 mm

Figure 4.1 Multidelamination Geometry [8]

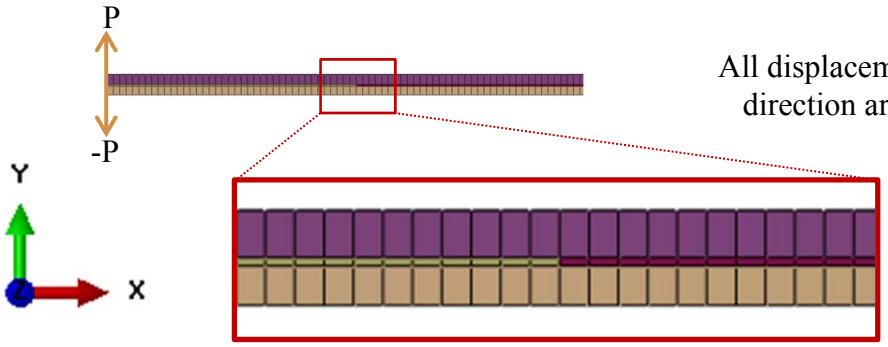

All displacements of nodes in width direction are constrained to zero

Figure 4.2 Multdelamination VCCT FE Model Geometry and Mesh

4.1.2 Mesh

The layers previously mentioned consist of C3D8R, reduced integration continuum elements. The middle section consists of one element in the width direction.

4.1.3 Material Properties

The material data [4, 8, 29] used for this study is shown below in Table 4.1 and Table 4.2.

Table 4.1 Bulk Material Properties for HTA913 Carbon Epoxy Composite (0_{24})

Bulk Material Properties for HTA913 Carbon-Epoxy Composite (0_{24})	
E_1	115.0 GPa
E_2	8.5 GPa
E_3	8.5 GPa
ν_{12}	0.29
ν_{13}	0.29
ν_{23}	0.3
G_{12}	4.5 GPa
G_{13}	3.3 GPa
G_{23}	4.5 GPa

Table 4.2 Material Data for Employment of VCCT

Material Data for Employment of VCCT	
G_{1c}	$0.33*10^3$ N/m
G_{2c}	$0.80*10^3$ N/m
G_{3c}	$0.80*10^3$ N/m
α	2
t_{01}	3.3 MPa
t_{02}	7.0 MPa
η	2.284

Where:
α= Ratio of Half Crack Length to Half Width of Specimen
t_{0i}= Strength of Interface
η= Exponent of Benzeggagh-Kenane (B-K) Law

4.1.4 Loads

The loading is shown above in Figure 4.2. The layered composite specimen is loaded by equal and opposite displacements in the thickness direction at one end. The maximum displacement is set equal to 40 mm in the monotonic loading case.

4.1.5 Boundary Conditions and Contact

All the nodes in the width direction are constrained to simulate the plane strain condition (Figure 4.2). Additionally, the applied loading nodes are constrained in the length direction. Lastly, contact is specified between the open faces of the second, pre-existing crack to avoid penetrations should the faces compress against one another during the analysis.

4.1.6 Virtual Crack Closure Technique Model Results

The data predicted using the VCCT agrees well with the experimental results presented in [4, 8, 29]. (See Figure 4.3.)

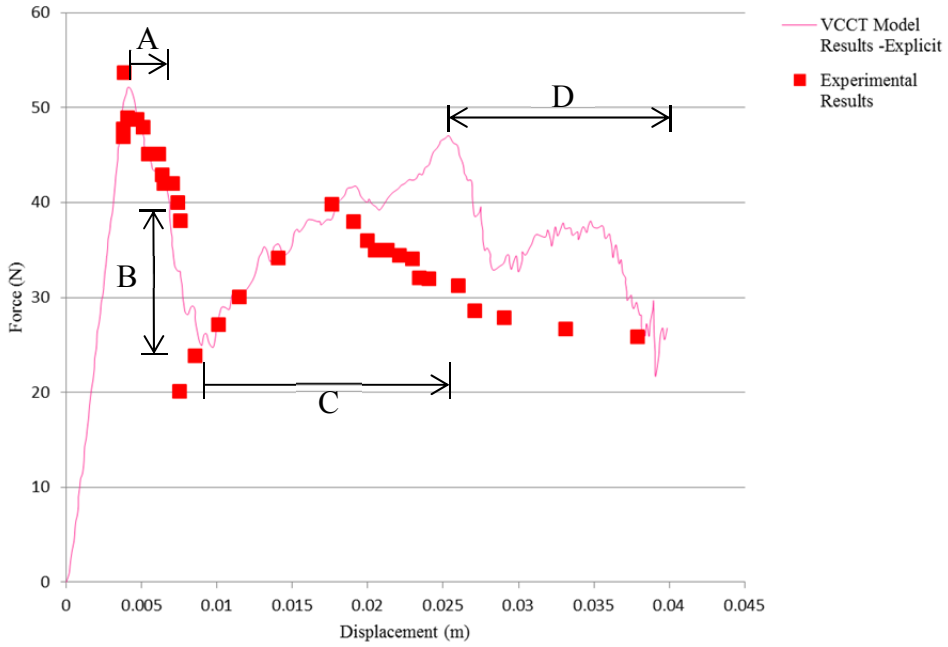

Figure 4.3 Experimental [8] and VCCT Model Results

Referring to Figure 4.3 above it can be seen that the main delamination grew in Zone A up to 4 mm, 52 N. Afterwards it can be noticed that it advanced a few millimeters before the start of the secondary delamination, at which it can be seen that there was an unstable jump of approximately sixteen millimeters (Zone B). Additionally, the main delamination is seen to be growing above the secondary delamination (seen in Zone C). Further, as this main delamination approached the end of the secondary delamination it grew in the direction of propagation of the initial delamination. Both of which eventually grew together leading to the main Zone D [29].

Note that the curve (Figure 4.3) obtained by applying the VCCT shows a discontinuous trend in the experimental data during the multiple delamination process. It

is of interest that the VCCT does not allow for a real simultaneous advancement of the first and second crack. Therefore, in order to avoid this hindrance, adaptive re-meshing processes should be used in each increment, increasing computational time [8].

4.2 Cohesive Elements Model

The CE Model (Figure 4.4 [4]) is the same as noted above for the VCCT model. However, there are a number of key differences. These are as follows:

1. The CE Model is modeled in three dimensions using solid elements to represent the bulk behavior and cohesive elements to capture the potential delamination at the interfaces between the tenth and eleventh layers and between the twelfth and thirteenth layers, from the bottom. (Figure 4.5).

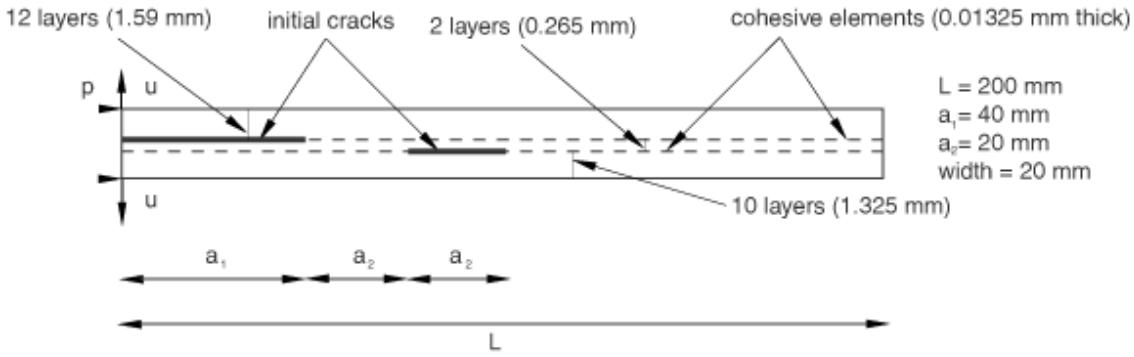

Figure 4.4 Multidelamination with CE Geometry [4]

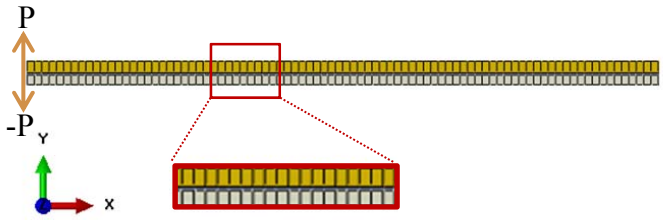

All displacements of nodes in width direction are constrained to zero

Figure 4.5 Multidelamination CE FE Model Geometry and Mesh

2. The initially un-cracked portions of the two interfaces are each modeled by one layer of COH3D8, 8-node three-dimensional cohesive elements that share nodes

with the adjacent solid elements. The top and bottom layer consists of C3D8R, reduced integration continuum elements. The middle section consists of one element in the width direction.

3. The response of the cohesive elements in the model is defined by the cohesive section definition as "traction-separation" response type.
4. The elastic properties of the cohesive layer material [4] are provided in terms of the traction-separation response with the stiffness values as appearing in Table 4.3:

Table 4.3 Elastic Properties of Cohesive Layer Material

Elastic Properties of Cohesive Layer Material	
E/E_{nn}	850 MPa/m
G_1/E_{ss}	850 MPa/m
G_2/E_{tt}	850 MPa/m

5. The quadratic traction-interaction failure criterion is selected for damage initiation in the cohesive elements; and a mixed-mode, energy-based damage evolution law based on a power law criterion is selected for damage propagation. The material data [4] pertinent to this is in Table 4.4.

Table 4.4 Material Data for Employment of CE

Material Data for Employment of CE	
N_0	3.3 MPa
T_0	7.0 MPa
S_0	7.0 MPa
G_{1c}	$0.33*10^3$ N/m
G_{2c}	$0.80*10^3$ N/m
G_{3c}	$0.80*10^3$ N/m
α	1.0

Where:
N_0= Ult. Strength I Direction
T_0= Ult. Strength II Direction
S_0= Ult. Strength III Direction
G_1, G_{2c}, and G_{3c} are the mode dependent energy release rates.
α= Exponent in Power Law

4.2.1 Cohesive Elements Model Results

The data predicted (Figure 4.6) relates well to the experimental results presented in [4]. A distinct drop in the reaction force is observed at 20 mm. Furthermore, the reaction force values seem to be under-predicted by approximately 30% in comparison with the experimental data in [4]. A reason for this deviation which happens to coexist with the synchronous generation of the first and second crack is related to a fairly large number of cohesive elements failing in an extremely short duration of time [4].

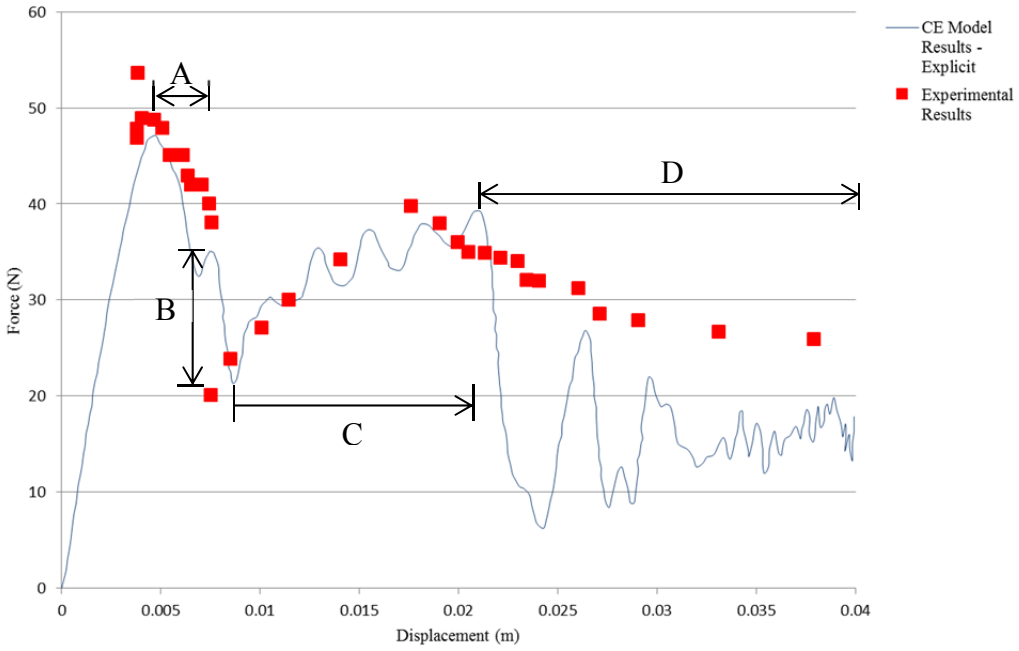

Figure 4.6 Experimental [8] and CE Model Results

Similar to Figure 4.3, it can be seen in Figure 4.6 that the main delamination grew in Zone A up to 5 mm, 48 N. Afterwards it can be noticed that it advanced a few millimeters before the start of the secondary delamination, at which it can be seen that there was an unstable jump of approximately fourteen millimeters (Zone B). Additionally, the main delamination is seen to be growing above the secondary delamination (seen in Zone C). Further, as this main delamination approached the end of

the secondary delamination it grew in the direction of propagation of the initial delamination. Both of which eventually grew together leading to the main Zone D [29].

For convenience the VCCT model results from Figure 4.3 are plotted with the CE model results from Figure 4.6 along with the experimental data below in Figure 4.7.

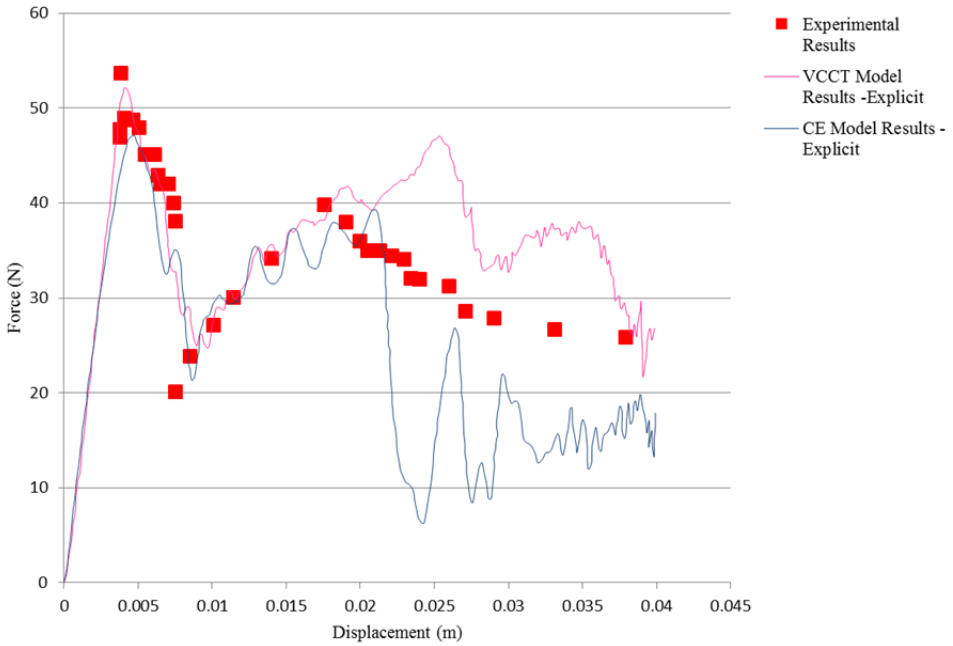

Figure 4.7 Experimental [8], VCCT Model, and CE Model Results

CHAPTER 5. ABAQUS/STANDARD MODEL

5.1 Structural Description

This study [1] considers a composite structure's flight-qualification testing. Part of which is a load-controlled test. Therefore, a representative composite assembly is loaded by a quasi-static axial compressive load which is monotonically increased until catastrophic failure occurs [1].

An adapter is used to join the load head and conic part. Further, there is an access door cut through the side of the conic (Figure 5.1).

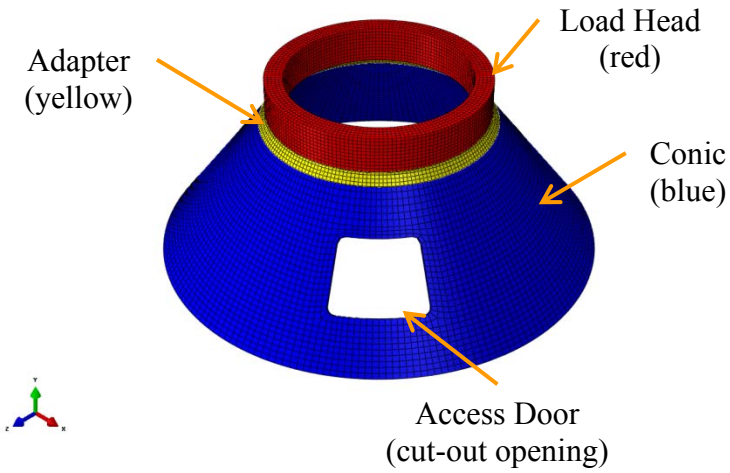

Figure 5.1 Composite Assembly

The conic part is a sandwich panel construction. The through-thickness profile of the sandwich panel (Figure 5.2 and Figure 5.3) is uniform in both the axial and hoop directions on the conic. The inner and outer composite faces of the sandwich

construction are a [(90/0)$_4$] layup as defined from the inside surface. Note that 0° is in the axial direction and 90° is in the hoop direction.

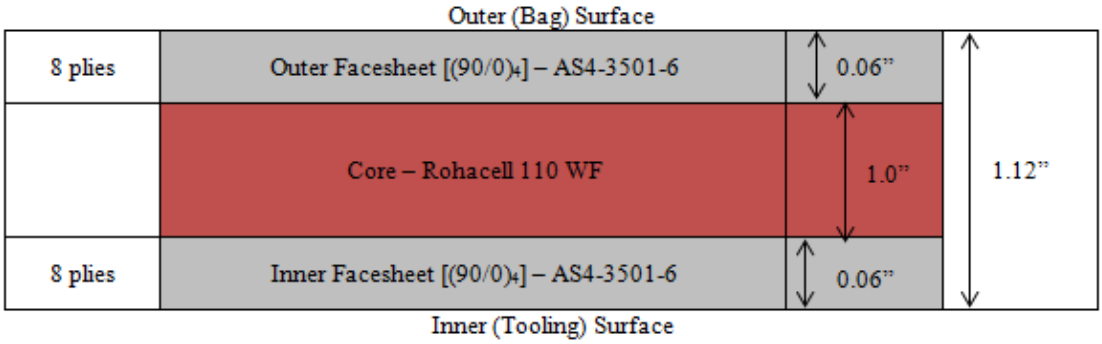

Figure 5.2 Composite Part Sandwich Panel Construction

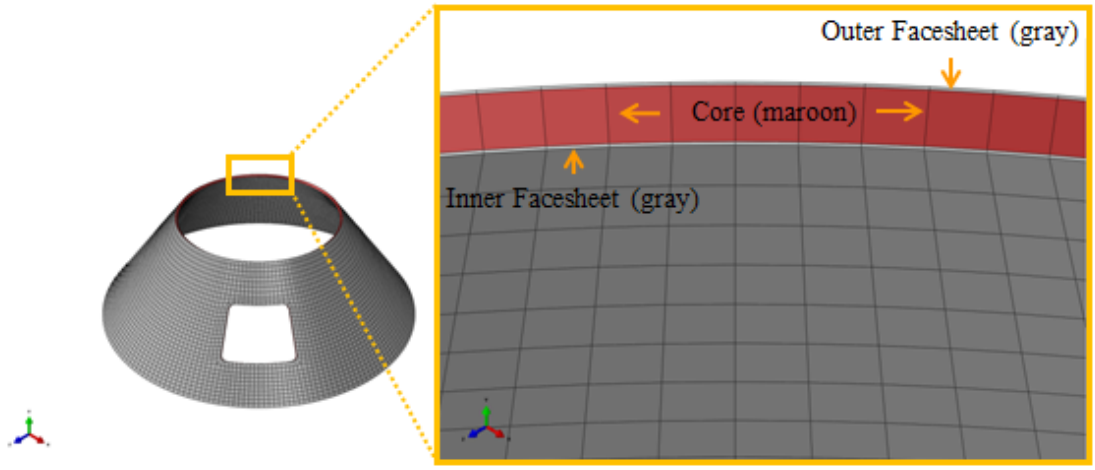

Figure 5.3 Composite Part Sandwich Panel Construction

5.2 Mesh

The load head and adapter are both meshed using C3D8R, Linear Hexahedral Elements. The conic is meshed using a combination of C3D8R, 8-node linear brick, reduced integration, hourglass control elements and C3D8RC3, 8-node linear brick, reduced integration, hourglass control, composite elements. Note that the C3D8RC3 Elements have only one integration point per ply. The mesh of this assembly can be seen in Figure 5.1.

5.3 Material Properties

In order to simplify the model, the adapter and load head are assumed to be rigid in comparison to the conic. As such, a large elastic modulus was chosen at random to designate the isotropic material used for both the adapter and load head (Table 5.1).

Table 5.1 Adapter and Load Head Material Properties

Rigid Material	
E	1 E 10 (psi)
ν	0.3

Each composite ply is 0.0075" thick and composed of carbon/epoxy AS4-3501-6. The 1" thick core is Rohacell 110 WF, an isotropic foam material. Material properties [1] for AS4-3501-6 and Rohacell 110 WF are in Table 5.2 and Table 5.3. A post failure stiffness ratio of 0.1 is used for matrix failure [1]. Meanwhile, a 0.01 post failure stiffness ratio is used for fiber failure [1].

Table 5.2 Conic Part Material Properties

AS4-3501-6		Rohacell 110 WF	
E_{11}	1.84 E 7 (psi)	E	2.61 E 4 (psi)
$E_{22} = E_{33}$	1.62 E 6 (psi)	ν	0.286
$\nu_{12} = \nu_{13}$	0.279	-	-
ν_{23}	0.531	-	-
$G_{12} = G_{13}$	9.51 E 5 (psi)	-	-
G_{23}	5.28 E 5 (psi)	-	-
S_{11}^{+}	2.83 E 5 (psi)	-	-
S_{11}^{-}	2.15 E 5 (psi)	-	-
$S_{22}^{+} = S_{33}^{+}$	6.96 E 3 (psi)	-	-
$S_{22}^{-} = S_{33}^{-}$	2.90 E 4 (psi)	-	-
$S_{12} = S_{13}$	1.15 E 4 (psi)	-	-
S_{23}	7.25 E 3 (psi)	-	-

Table 5.3 AS4-3501-6 Constituent Properties

Fiber		Matrix	
E_{11}	3.06 E 7 (psi)	E_{11}	3.95 E 5 (psi)
$E_{22} = E_{33}$	2.46 E 6 (psi)	$E_{22} = E_{33}$	6.84 E 5 (psi)
$\nu_{12} = \nu_{13}$	0.247	$\nu_{12} = \nu_{13}$	0.323
ν_{23}	0.197	ν_{23}	0.486
$G_{12} = G_{13}$	2.62 E 6 (psi)	$G_{12} = G_{13}$	3.55 E 5 (psi)
G_{23}	1.03 E 6 (psi)	G_{23}	2.30 E 5 (psi)

5.4 Loads

In this composite assembly's flight-qualification testing four actuators deliver vertical compressive point loads to the load head (Figure 5.4).

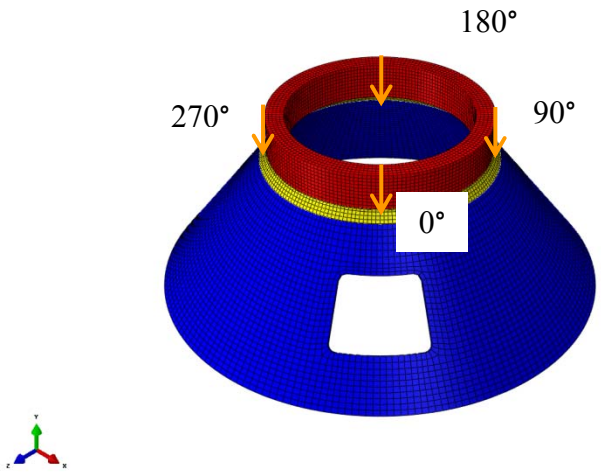

Figure 5.4 Composite Assembly Loading

The compressive loads [1] applied at four locations on the load head are shown in Table 5.4.

Table 5.4 Load Head Compressive Forces

Load	Actuator Azimuth				Total Load
	000	090	180	270	
0%	0 kips	0 kips	0 kips	0 kips	0 kips
50%	-250 kips	-250 kips	-250 kips	-250 kips	-1000 kips
100%	-500 kips	-500 kips	-500 kips	-500 kips	-2000 kips

Note that the loading is linearly ramped and is quasi-static. Also, a negative sign demonstrates a compressive load. These loads produce a uniform vertical compressive load where 100% loading correlates to a cumulative vertical compressive load of 2000 kips.

5.5 Boundary Conditions

The composite assembly is constrained by its entire bottom surface using a fixed boundary condition (Figure 5.5). Therefore, displacements and rotations in the one, two, and three directions are constrained to be zero.

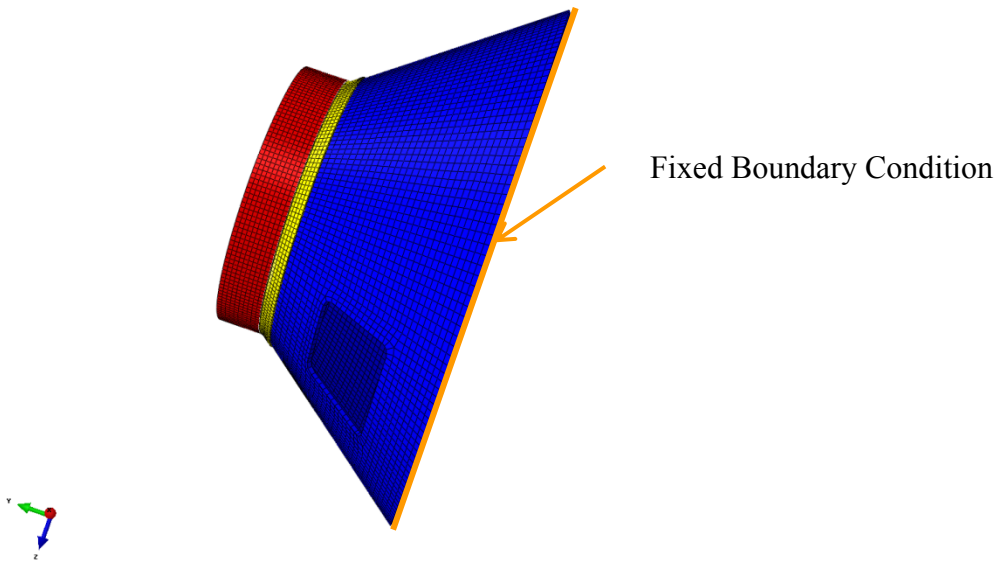

Figure 5.5 Composite Assembly Boundary Condition

CHAPTER 6. MODEL COMPARISON

6.1 Linear Elastic Analysis

Abaqus/Standard has a three-dimensional continuum element, C3D8R (reduced integration element), which can use a multilayer composite lay-up. Continuum elements record all six stress components (σ_{11}, $\sigma_{22,}$ σ_{33}, σ_{12}, $\sigma_{13,}$ σ_{23}) which allow the material failure criteria to use the transverse stress components (σ_{33}, $\sigma_{13,}$ σ_{23}). These are only estimated in conventional or continuum shell elements. The importance of recording transverse stress components is demonstrated by a linear elastic analysis. This analysis allows for the juxtaposition of magnitudes of the in-plane and transverse stress components in the greatest stressed region of the model. The FE Model for this analysis is as described before. It is worth mentioning that the element type is C3D8R and the through-thickness mesh density for both the composite facesheets and foam core is one element [1].

6.1.1 Linear Elastic Analysis Results

The results are presented for the stress state of element 5240 (Table 6.1 and Figure 6.1-Figure 6.6). This element lies in the topmost surface ply near the left-hand corner of the access door of the assembly. Fiber failure is dependent on the stress components: σ_{11}, σ_{12}, σ_{13}. Upon closer inspection it can be seen that the transverse shear stress, σ_{13}, is negligible when compared to the in-plane stresses. As such, transverse

stresses will not donate a notable contribution to fiber failure. Conversely, matrix failure is propelled by all six stress components. Through the comparison of the magnitude of the out-of-plane stresses: σ_{33}, σ_{13}, σ_{23} with the magnitude of the in-plane stresses: σ_{22}, σ_{12}, it can be noted that the out-of-plane stresses contribute significantly to matrix failure. After a matrix failure the matrix stiffness significantly drops and the stress is redistributed. This subsequently causes an increase in stress in the fibers. Therefore, in order to most accurately predict structure-level failure, matrix failure must be appropriately captured [1].

Table 6.1 Linear Elastic Analysis Results

Stress Component	Value (psi)	Normalized ($\lvert\sigma_{ij}/\sigma_{11}\rvert$)	Normalized ($\lvert\sigma_{ij}/\sigma_{22}\rvert$)	Normalized ($\lvert\sigma_{ij}/\sigma_{12}\rvert$)
σ_{11}	-260,063	100.0%	4245.2%	1548.6%
σ_{22}	-6,126	2.4%	100.0%	36.5%
σ_{33}	780	0.3%	12.7%	4.6%
σ_{12}	16,793	6.5%	274.1%	100.0%
σ_{13}	-352	0.1%	5.7%	2.1%
σ_{23}	945	0.4%	15.4%	5.6%

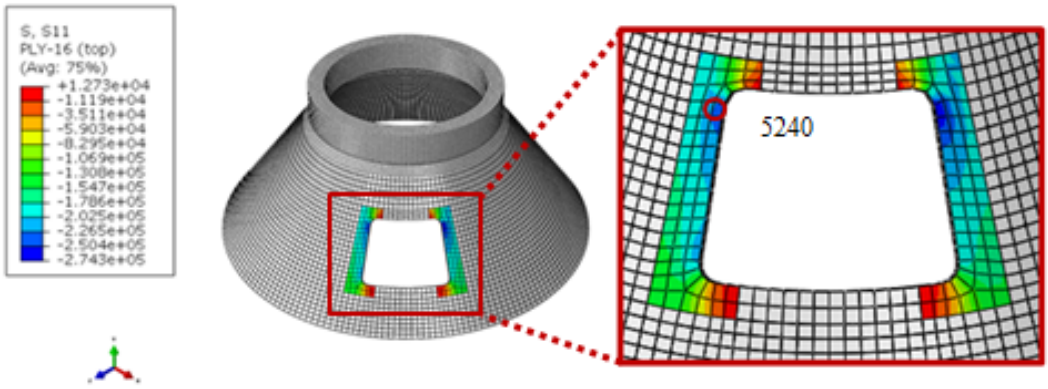

Figure 6.1 σ_{11} Linear Elastic Analysis Results

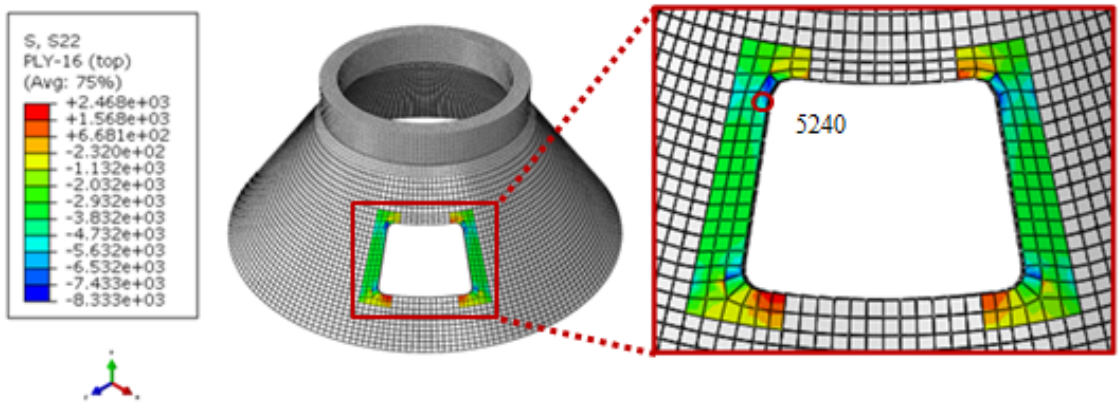

Figure 6.2 σ_{22} Linear Elastic Analysis Results

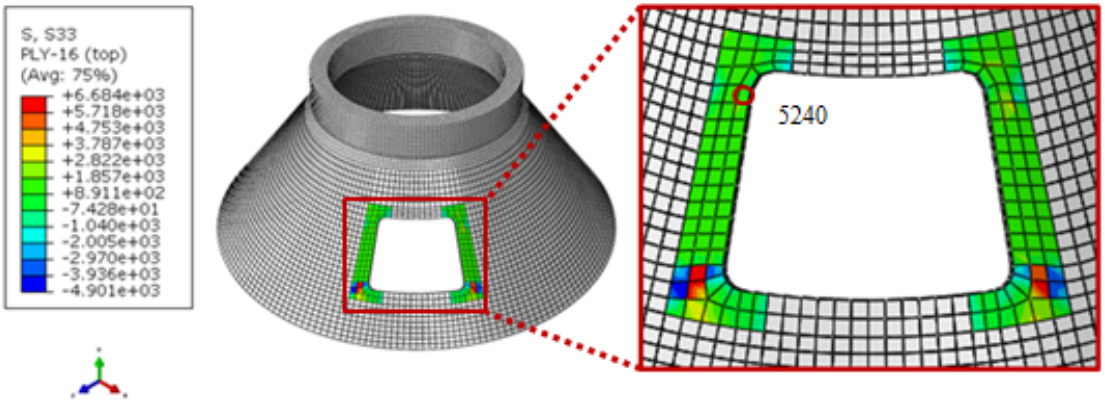

Figure 6.3 σ_{33} Linear Elastic Analysis Results

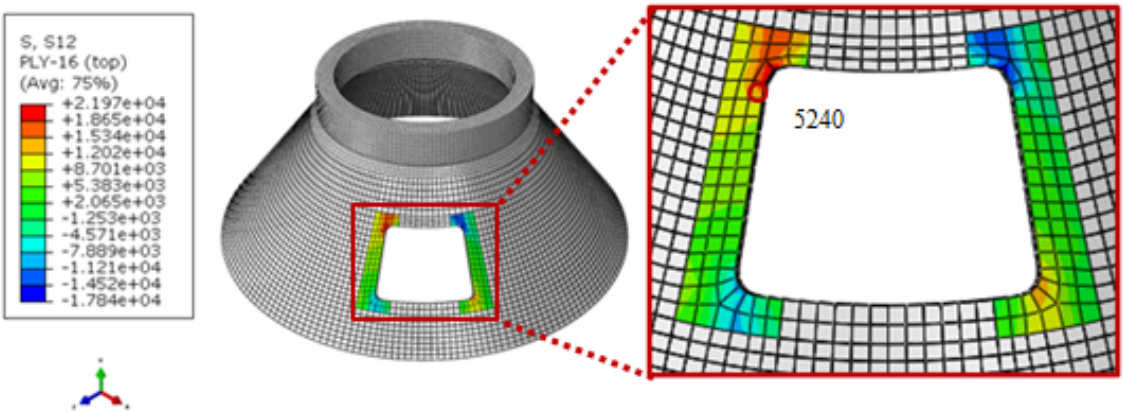

Figure 6.4 σ_{12} Linear Elastic Analysis Results

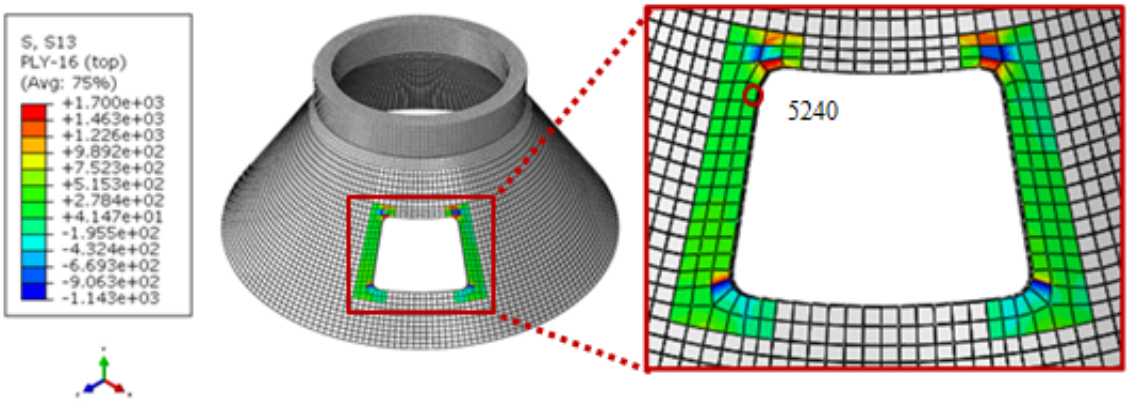

Figure 6.5 σ_{13} Linear Elastic Analysis Results

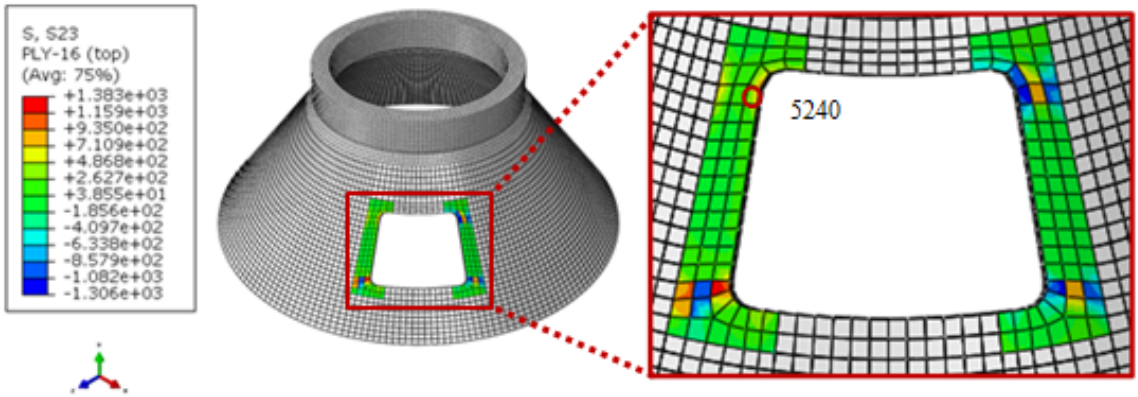

Figure 6.6 σ_{23} Linear Elastic Analysis Results

6.2 First Failure Analysis

An analysis is performed to examine first failure. An initial endeavor at a progressive failure analysis explicitly consists of a through-thickness mesh density of one element per facesheet and one element for the core. This is a total of three elements through the thickness of the sandwich construction. In this case, the C3D8R (reduced integration element) is used. This first failure analysis will provide a base-line estimate that will be used for correlating further modeling attempts [1].

6.2.1 First Failure Analysis Results

Table 6.2 shows the load level at which matrix failure, fiber failure, or global failure is predicted respectively.

Table 6.2 First Failure Analysis Results

Model	Element Type	#Elements (Facesheet)	#Elements (Core)	Matrix Failure (Load Level)	Fiber Failure (Load Level)	Global Failure (Load Level)
1 Element Face_1 Element Core	C3D8R	1	1	49%	57%	58%

The prediction of failure is based on the Multicontinuum Theory (MCT) Failure Criterion presented in Chapter 3, Section 3. Please note that the table indicates at which load the localized fiber or matrix failure is first detected. The first occurrence of a fiber or matrix failure happens at a single Gaussian integration point within one of the material plies of an element in the model. In a large composite assembly containing many Gaussian integration points, an overwhelming number of localized constituent failures are needed to detect a distinct alteration in the global stiffness of the assembly [1].

Assembly global failure is determined for this study to be a significant discontinuity (large drop) in the overall vertical load-displacement curve (Figure 6.7 below).

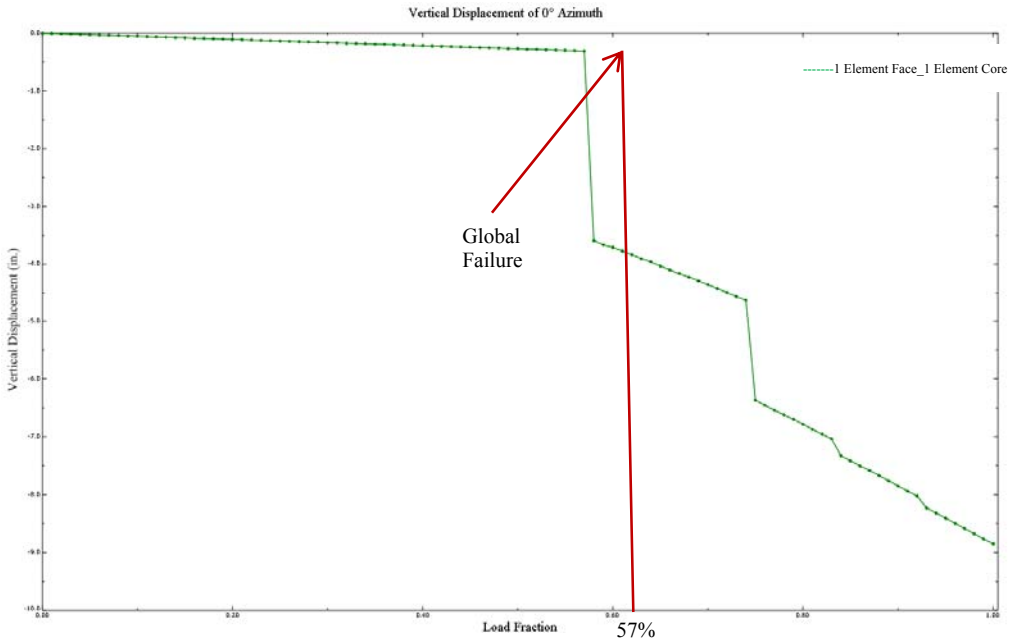

Figure 6.7 First Failure Analysis Results

Overall the vertical deformation is evaluated using the vertical displacement at the load head labeled 0° (Node 17). Since, both the load head and adapter are assumed rigid, a large discontinuity witnessed in the load-displacement curve hints at an accelerated growth of localized material failures occurring during a distinct load increment [1]. Thus, degradation in the overall stiffness of the composite assembly can be witnessed.

Figure 6.7 shows this overall vertical load-deflection curve. It should be noted that the cumulative response of the assembly looks linear to load level 57%. At this load level global failure occurs. Referring to Table 6.2 it is noticed that the first localized matrix failure occurs at a load level of 49% and conversely the first localized fiber failure occurs at a load level of 57%. The localized failures that occurred in the range from 49% to 57% were not adequate in producing a noticeable difference in the assembly's overall load-deflection response. However, when the load level was increased from 57% to 58% subsequent failures occur. These continuous failures that occur significantly reduce the

vertical stiffness of the assembly by 92%. This behavioral response, in which the composite assembly stays fairly linear up to global failure, is typical among brittle composite materials [1].

6.3 Effect of Through-Thickness Mesh Density

The prediction of progressive failure response of the conical composite is performed through the use of four separate FE models. The models differ in the number of elements through the thickness of the sandwich panel. For example, the materials, element type, in-plane mesh density, and boundary conditions for all four models are the same. The different levels of through-thickness mesh density are the following [1]:

1. Initial model – 1 element per facesheet for the entire layup and 1 element for the core (3 elements through-thickness).
2. 1st Modification – Core mesh density increased to allow for 4 elements (6 elements through-thickness).
3. 2nd Modification – Facesheet mesh density increased to allow for 2 elements (8 elements through-thickness).
4. 3rd Modification – Facesheet mesh density increased to allow for 4 elements (12 elements through-thickness).

Note that each of the four models uses C3D8R reduced integration elements.

6.3.1 Effect of Through-Thickness Mesh Density Results

Table 6.3 below shows the load level at which the matrix, fiber, and global failures are predicted for the four separate FE models.

Table 6.3 Through-Thickness Mesh Density Failure Analysis Results

Model	Element Type	#Elements (Facesheet)	#Elements (Core)	Matrix Failure (Load Level)	Fiber Failure (Load Level)	Global Failure (Load Level)
1 Element Face_1 Element Core	C3D8R	1	1	49%	57%	58%
1 Element Face_4 Element Core	C3D8R	1	4	48%	61%	64%
2 Element Face_4 Element Core	C3D8R	2	4	52%	60%	60%
4 Element Face_4 Element Core	C3D8R	4	4	59%	60%	60%

Figure 6.8 below shows the overall vertical load-displacement curves for the four separate FE models considered in this through-thickness mesh density study for the composite assembly.

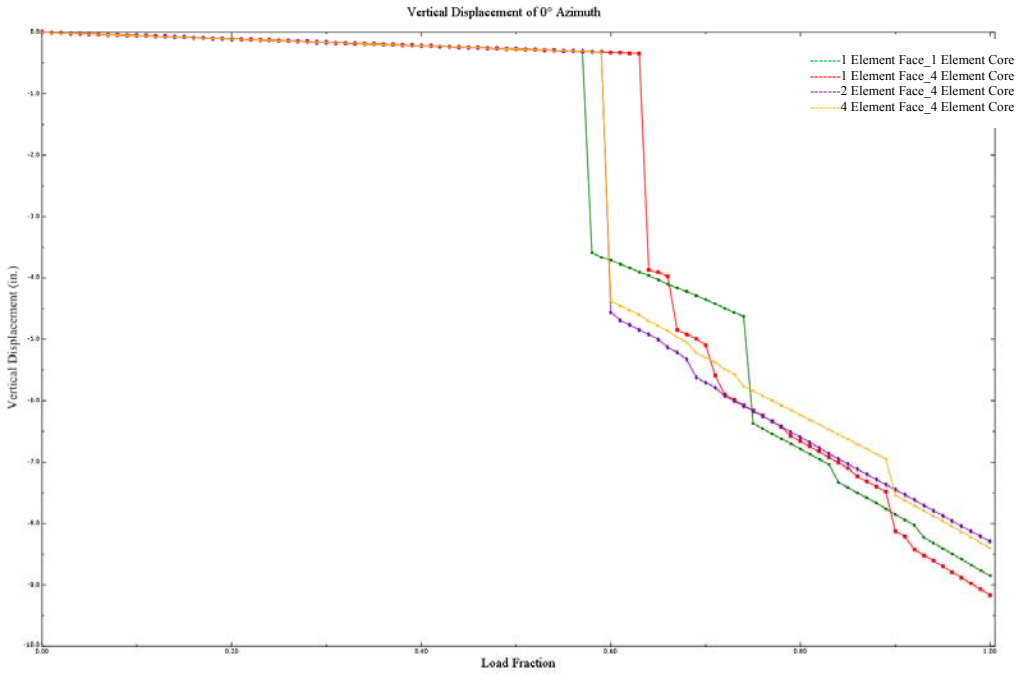

Figure 6.8 Through-Thickness Mesh Density Failure Analysis Results

Observations can be made from the above results. First, commencement of localized matrix and fiber failure is estimated at higher load levels as the through-thickness mesh density is increased. As the number of elements through the thickness of the laminate is increased the transverse shear stiffness of the assembly decreases quicker than the in-plane stiffness. Therefore, as the through-thickness mesh density is increased, the assembly exhibits an increase in transverse shear deformation at the cost of in-plane deformation. As such, the net outcome of this tendency is that the magnitude of the in-plane stresses at their peaks tends to decrease as the through-thickness mesh density increases. Thus, higher load levels are predicted for localized failure [1].

Second, mesh density does not have an extreme affect on global failure. Even though it was shown that through-thickness mesh density contributes to slower local failure initiation for both the fiber and matrix, the global failure prediction is only slightly

affected. This suggests, that the subsequent failures from local failure to global failure occurs quicker as the through-thickness density is increased. It is then expected that local failures progress into global failures at a quicker rate for a higher mesh density. As such, a denser mesh allows for a more defined failure path for an assembly. This is for the reason that the number of Gaussian integration points has been increased for failure criterion evaluation. Thus, a more defined path allows for a quicker progression of failure and consequently an accelerated progression of local failures into global failures [1].

6.4 Effect of Element Type

The prediction of the progressive failure response of the conical composite is further considered through the use of three FE models. The models differ in element type used. Expressly stated, the materials, mesh density, and boundary conditions are explicitly the same in each model. Three different Abaqus element types were considered [1]:

1. C3D8R, 8-node linear brick, hourglass control, reduced integration continuum elements
2. C3D8, 8-node linear brick, fully integrated continuum elements
3. SC8R, 8-node quadrilateral in-plane general-purpose reduced integration continuum shell, finite membrane strains

The three models all use four elements for the core and each facesheet is divided into two elements. This creates a total of eight elements through the thickness of the sandwich panel.

6.4.1 Effect of Element Type Results

Table 6.4 below shows the load level at which the matrix, fiber, and global failures are predicted for the three separate FE models.

Table 6.4 Element Type Failure Analysis Results

Model	Element Type	#Elements (Facesheet)	#Elements (Core)	Matrix Failure (Load Level)	Fiber Failure (Load Level)	Global Failure (Load Level)
2 Element Face_4 Element Core	C3D8R	2	4	52%	60%	60%
C3D8	C3D8	2	4	41%	47%	56%
SC8R	SC8R	2	4	42%	62%	72%

Figure 6.9 below shows the overall vertical load-displacement curves for the three separate FE models considered in this element type study for the composite assembly.

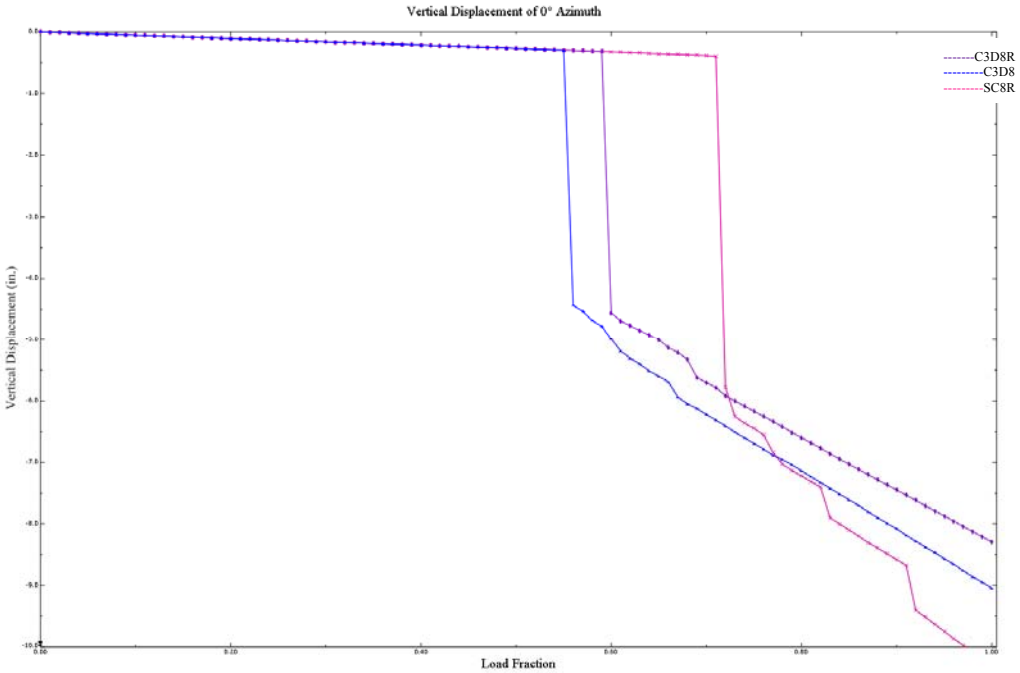

Figure 6.9 Element Type Failure Analysis Results

Comparing the C3D8R elements vs. C3D8 elements allows for a couple of observations to be made. First, the C3D8 element exhibits both matrix and fiber local failure occurrences happening at lower load levels. Additionally, the C3D8 element uses more Gaussian integration points when compared with the C3D8R element. If both elements result in the same element average stresses, the C3D8 element will show a higher local peak stress than the C3D8R element. This is for the reason that it has a greater amount of Gaussian integration points and whose Gauss points are closer to the element's boundaries. Recall that at an element's boundaries the linear stress distribution reaches maxima. Therefore, the C3D8 element will show localized failure initializing at a lower load level than that of the C3D8R element [1].

Second, the C3D8 element shows global failure occurring at a lower load level. The difference in the global failure prediction by the two different elements is primarily due to the differences in the local failure commencement load. It is important to recall that a C3D8R element has a single Gauss point per material ply. This provides a more discretized representation of subsequent failure. For example, when failure occurs in a material ply of a C3D8R element, the stiffness of the whole ply is reduced and there is a large quantity of load re-distribution. However, in an example when failure occurs at one of the Gauss points in a material ply of a C3D8 element, only a portion of the material ply encounters the stiffness reduction and as a consequence only a small quantity of load re-distribution [1].

Additional observations can be made in comparing the C3D8R elements with the SC8R elements. First, the SC8R elements predict the initialization of local failure at 42 % load level compared to the C3D8R elements at 52% load level. Recall that both elements

use the same group of Gaussian integration points. However, the SC8R elements predict higher in-plane stress components than that of the C3D8R elements. This is because of the differences in the transverse shear stiffness and transverse normal stiffness of the two elements. The C3D8R element has transverse stiffness which is a result of integrating the individual material plies over the volume of the element. Meanwhile, the SC8R element has transverse stiffness as the result of a user input that applies to the entire element. This inhibits the ability for both elements to have identical transverse stiffness. Therefore, any alteration in the transverse stiffness of an element will conclude in a division of the element's total strain energy into in-plane and out-of-plane components differently for the two elements. As such, if the two elements have distinct transverse stiffness, they will have distinct in-plane stress components. In regard to this study, the initial matrix failure is a consequence of in-plane shear stress which is greater in the SC8R element than in the C3D8R element. Thus, the SC8R element predicts localized matrix failure earlier [1].

Second, continuum shell elements show global failure to occur at a higher load level despite local failures occurring at lower load levels. The SC8R element shows local constituent failure initiating at a lower load level than that of the C3D8R element. However, despite this, the SC8R element shows that global failure will occur at 72% load level compared to the 60% load level of the C3D8R element. The reason for the SC8R element predicting a slower failure is because the local material failures do not alter the transverse stiffness (E_{33}, G_{13}, G_{23}) in the SC8R element. (Recall here that it is a requirement in Abaqus that these stiffness values are constant in the SC8R element.) [1]. Therefore, the transverse stiffness does not exhibit any degradation. The SC8R elements

can readily welcome load re-distribution without influencing further local failures. Thus, it is noticed that the C3D8R and SC8R elements show a substantial difference in failure behavior [1].

CHAPTER 7. COMPARISON OF FINITE ELEMENT APPROACHES

Two commercially available FE analytical tools will be discussed and compared in terms of their failure criteria and progressive damage results. These analytical tools are Abaqus/Standard and Helius PFA 2016. Note that Helius PFA is a plugin for Abaqus and uses a parallel pre-processor; however, Helius does use Abaqus' solver. Figure 7.1 below provides a high-level flowchart regarding the interaction of these tools.

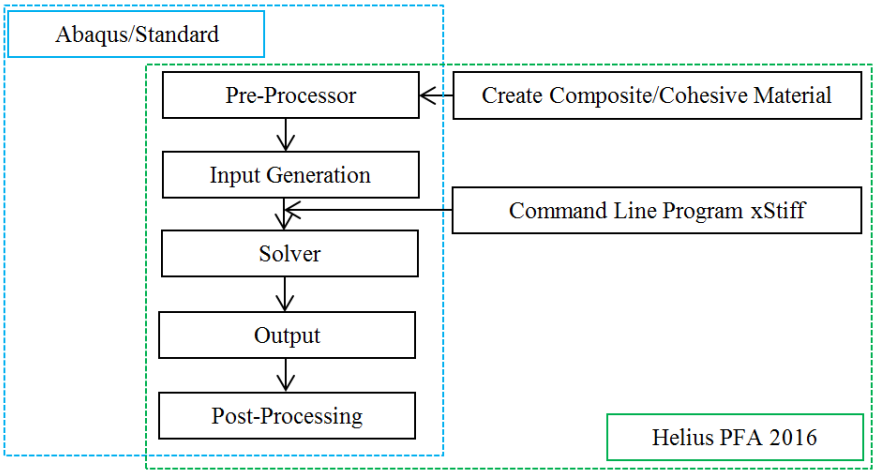

Figure 7.1 Abaqus/Standard and Helius PFA 2016 Relationship Flowchart

7.1 Results Using Linear Elastic Abaqus Failure Criteria and Helius PFA's MCT Criterion

Abaqus/Standard provides five failure criteria to use in linear elastic analyses. Four of these failure criteria are stress-based and the remaining criterion is strain-based. The ability to use these failure criteria is limited due to the fact that they only anticipate

the incidence of localized failure not global failure. Otherwise put Abaqus' failure criteria do not predict an accompanying stiffness reduction after a failure occurs. Therefore, it does not capture progressive failure. However, a software plugin to Abaqus, Helius PFA (through its MCT criterion) predicts both localized failure and an accompanying stiffness reduction. Furthermore, the homogenized composite state of stress or strain is used to anticipate failure of a homogenized material in Abaqus' linear elastic failure criteria while the MCT criterion uses constituent average stress to independently anticipate failure of each constituent [1, 4].

In the composite assembly examined here, it can be assumed that the material is linearly elastic leading up to global failure. In this regard, the onset of failure can be compared between Abaqus' linear elastic failure criteria and the MCT criterion. The failure criteria provided by Abaqus are generally applied to orthotropic materials; however, for this assembly a transversely isotropic material is used for both Abaqus' linear elastic failure criteria and the MCT criterion. It should be noted that Abaqus' linear elastic failure criteria is based on a presumed condition of plane stress. This is a hindrance as these failure criteria can then only be used in a plane stress state with 2-D continuum or shell elements. On the other hand, the MCT criterion uses these elements and a 3-D state of stress in SC8R elements in its applicable failure criteria [1, 4]. These are used in the results presented below as to form a more direct comparison with the shortcomings of Abaqus' linear elastic failure criteria.

In general for composite laminates, laminate failure is said to be first ply failure. To be concise, only Abaqus' Maximum Stress criterion and Tsai-Wu failure criterion (both stress-based criteria) are compared with Helius PFA's MCT failure criterion.

Table 7.1 below shows the predicted load level for each type of failure using Maximum Stress, Tsai-Wu, and MCT respectively.

Table 7.1 Linear Elastic Failure Analysis Results

Model	Criterion	Element Type	#Elements (Facesheet)	#Elements (Core)	Matrix Failure (Load Level)	Fiber Failure (Load Level)	Global Failure (Load Level)
Stress Based Failure	Max Stress	SC8R	2	4	43%	43%	N/A
	Tsai-Wu	SC8R	2	4	45%	45%	N/A
SC8R	MCT	SC8R	2	4	42%	62%	72%

Figure 7.2 shows the vertical load-displacement curves for the load application location of 0° on the load head.

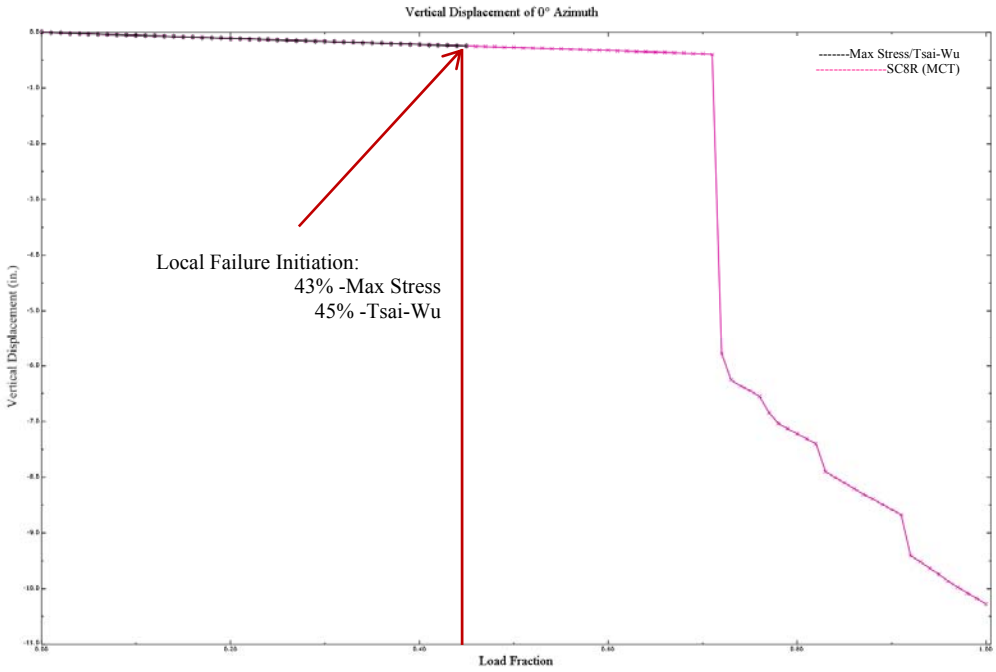

Figure 7.2 Linear Elastic Failure Analysis Results

It can be seen from Figure 7.2 that before global failure is achieved at 72% load level both Abaqus' linear elastic failure criteria and the MCT criterion predict similar

overall structural stiffness. As such it is important to recall that using the linear elastic material failure criteria; the material stiffness reduction is not considered. In this manner, the failure analysis is only able to be run up to the instance when localized failure initiation is predicted. However, the MCT criterion has the advantage to reduce material stiffness at integration points that have failed (both matrix and fiber) which then can be used to accurately predict the advancement of local failure initiation into global failure. Here it is imperative to recall that a composite structure has the ability to retain the majority of its structural stiffness beyond the instance of local failure initiation. Furthermore, composite designs based off of first-ply failure tend to be over-conservative in nature and the full capability of the composite is not understood. Thus, in this circumstance, it is advantageous to use the MCT criterion in the prediction of global failure as the description of post-failure behavior of this composite assembly is not available within Abaqus' linear elastic failure criteria [1].

7.2 Results Using Abaqus' Progressive Damage and Helius PFA's MCT Criterion

Progressive damage modeling is accomplished in Abaqus through the use of the Hashin criterion. The Hashin criterion predicts the initiation of four different constituent failure modes (tensile fiber failure, compressive fiber failure, tensile matrix, and compressive matrix failure) and uses damage evolution equations to predict the stiffness reduction which is a result of the evolution of damage from these modes [1].

It is important to note the many differences between Abaqus' progressive damage model and the instantaneous progressive failure model that is available via Helius PFA. They are as follows [1]:

1. In the Hashin criterion the material stiffness is reduced slowly as deformation accumulates after the initiation criterion has been met. Meanwhile, in the MCT criterion a rapid stiffness reduction is driven by the constituent that failed.
2. In the Hashin criterion, damage initiation and evolution of both the matrix and fiber constituents are predicted using the composite average states of stress and strain. However, in the MCT criterion the constituent average stress states are used to predict failure in the individual constituents, both matrix and fiber.
3. In the Hashin criterion, the prediction of damage initiation and evolution is based on the in-plane stress and strain components. The additions of the transverse stress and strain components are ignored. This is not the case in the MCT criterion. MCT predicts the constituent failure using a 3-D constituent average stress state.
4. In the evolution of progressive damage in the Hashin criterion the stiffness reduction is only accounted for in the in-plane stiffness (E_{11}, E_{22}, G_{12}). This leaves the transverse stiffness (E_{33}, G_{13}, G_{23}) unaltered. However, the MCT criterion allows for stiffness reduction in both the in-plane and transverse stiffness.
5. Lastly, progressive damage modeling through the Hashin criterion is only available with the use of 2-D continuum elements and shell elements. In contrast, the MCT criterion can use both of these element types as well as 3-D continuum elements.

In regard to the composite assembly examined here, the Hashin criterion and MCT criterion are each used to simulate failure. It is for reason four and reason five stated above that SC8R elements are used in the Hashin criterion and MCT criterion.

Therefore, the differences expressed in reasons four and five can now be neglected. Therefore, any differences captured between the results of the Hashin criterion and the MCT criterion are due to the differences expressed in reasons one through three above.

In the Hashin criterion after the first localized matrix failure happened a converged solution could not be obtained. As a result, the data documented here does not include a global failure through the use of the Hashin criterion. Table 7.2 below shows the predicted load level for each type of failure using the two different progressive damage models after local matrix failure. Note that by turning off *DAMAGE EVOLUTION in the Abaqus progressive damage model and using the Hashin criterion to flag matrix and fiber failure, neglecting the reduction in the material stiffness after local failure, it is possible to approximately conclude when fiber failure would occur. It is important to state that this value is approximate since a material stiffness reduction due to local matrix failure has the ability to cause fiber failure to initiate early [1].

Table 7.2 Progressive Damage Failure Analysis Results

Model	Criterion	Element Type	#Elements (Facesheet)	#Elements (Core)	Matrix Failure (Load Level)	Fiber Failure (Load Level)	Global Failure (Load Level)
Hashin	Hashin	SC8R	2	4	50%	75%	N/A
SC8R	MCT	SC8R	2	4	42%	62%	72%

Table 7.2 presents and Figure 7.3 below shows that the Hashin criterion's prediction of localized matrix failure occurs at 50% load level compared to the 42% load level as predicted by the MCT criterion. This difference can be explained. It is largely due to the differences that are inherent to the matrix constituent failure criteria used by

the Hashin and MCT criterion respectively. Explicitly, the difference is the composite average stress vs. the constituent average stress and the stress-based failure criterion used in each model [1].

It can be seen that the Hashin criterion predicts the first localized fiber failure to occur at load level 75%. However, the MCT criterion predicts the first localized fiber failure to occur at 62% load level. This discrepancy in the load level of local fiber failure initiation is the result of two primary reasons. The first reason is that the Hashin criterion uses the homogenized composite average stress state. Meanwhile, the MCT criterion uses the fiber average stress state. The second reason is that the MCT criterion predicts an instantaneous stiffness reduction with localized matrix failure. As such, the load is re-distributed to the fibers at a quicker rate than the Abaqus progressive damage evolution model, Hashin criterion, predicts [1].

An interesting observation to note from Figure 7.3 is that the Hashin criterion predicts localized fiber failure to occur at load level 75%. However, MCT predicts global failure to occur at load level 72%. In this case, an emphasis should be made on the fact that after localized matrix failure begins; a converged solution for Abaqus' progressive damage model could not be obtained. Therefore, global failure could not be determined. Thus, the turning off of *DAMAGE EVOLUTION and using the Hashin criterion to flag matrix and fiber failure to ultimately determine when fiber failure would occur is most likely responsible for the increased load level related to the localized fiber failure load levels [1].

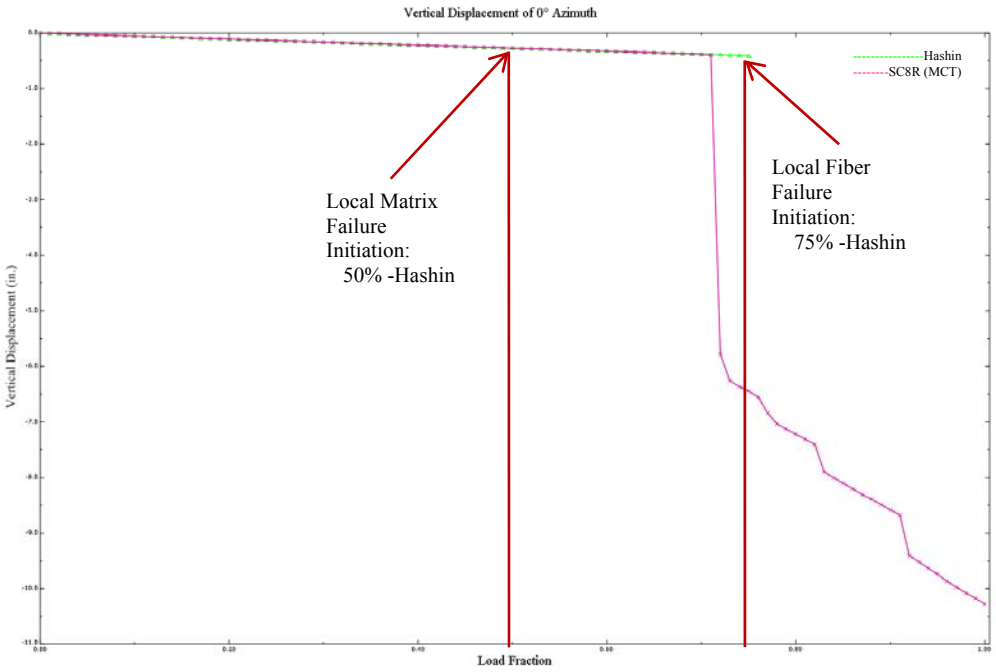

Figure 7.3 Progressive Damage Failure Analysis Results

7.3 Comparison of Liner Elastic Failure Analysis Results vs. Progressive Damage Failure Analysis Results

Table 7.3 and Figure 7.4 below provide the data and the vertical load-displacement plot for Abaqus' Max Stress Criterion, Tsai-Wu Criterion, and Helius PFA's MCT criterion, respectively.

Table 7.3 Comparison of Linear Elastic Failure Analysis Results vs. Progressive Damage Failure Analysis Results

Model	Criterion	Element Type	#Elements (Facesheet)	#Elements (Core)	Matrix Failure (Load Level)	Fiber Failure (Load Level)	Global Failure (Load Level)
Stress Based Failure	Max Stress	SC8R	2	4	43%	43%	N/A
	Tsai-Wu	SC8R	2	4	45%	45%	N/A
Hashin	Hashin	SC8R	2	4	50%	75%	N/A
SC8R	MCT	SC8R	2	4	42%	62%	72%

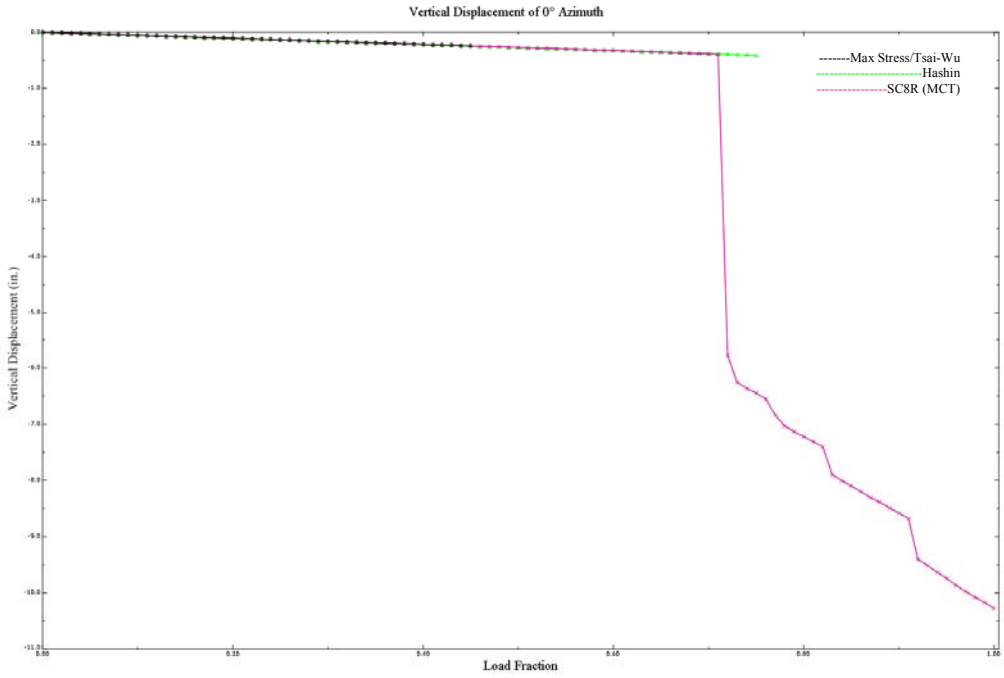

Figure 7.4 Comparison of Linear Elastic Failure Analysis Results vs. Progressive Damage Failure Analysis Results

It is interesting to observe the overlay of these failure theories. In doing so, it can be observed: First, Abaqus' stress-based criteria are only viable until localized failure initiation is predicted. This introduces over-conservatism into the composite design. Second, Abaqus' progressive damage model did not converge to a solution. Data could only be reported for the Hashin Criterion through Abaqus if matrix and fiber failures were flagged and reduction in material stiffness after local failure was neglected. This created approximation tends to predict fiber failure to initiate early. Lastly, Abaqus' progressive damage model is not able to predict an instantaneous stiffness reduction with local matrix failure. As a result, the load is re-distributed to the fibers at a slower rate. Thus, the fiber failure load level is over-predicted.

CHAPTER 8. CONCLUSION

This paper has presented a composite structure used in flight-qualification testing. This structure's overall load-displacement response has been characterized. It has been found that Abaqus/Explicit is able to predict mixed-mode multidelamination in a layered composite specimen through both the VCCT and CE fairly close to the results obtained in experimental test in literature. Further, a thorough comparison has been provided in which the effects of failure criteria type, through-thickness mesh density, and finite element type on the progressive failure response of this composite assembly have been discussed. Lastly, Abaqus/Standard and Helius PFA were compared in order to gain confidence into the capabilities of these analytical models in determining different scales of failure (local/microscale and global/macroscale).

CHAPTER 9. FUTURE WORK

It is of interest to explore further topics related to those presented herein. It would be worthwhile to pursue the following:

1. A study on the similarities and differences associated with short and long fiber composites (i.e. Scale Dependent Analyses).
2. A study is performed in Abaqus/Explicit in which mixed-mode multi/delamination is predicted through the use of VCCT and CE for a short fiber composite.
3. A study performed in Abaqus/Explicit in which mixed-mode multi/delamination is predicted through the use of the Extended Finite Element Method (XFEM) via short and long fiber composites.
4. The effect of failure criteria type, through-thickness mesh density, and finite element type on the progressive failure of this conical composite is considered using a short fiber composite.
5. A comparison is done for short and long fibers composites for the work presented herein and that obtained from above.

REFERENCES

REFERENCES

[1] Autodesk, "Autodesk Helius PFA 2016," 2016. [Online]. [Accessed 4 August 2016].

[2] J. San-Millan, "Delamination and Debonding Grwoth in Composite Structures," *Springer Link,* pp. 63-88, 2015.

[3] G. E. Sanford, "Failure Testing of Large Composite Aerospace Structures," ICCM-Central, [Online]. Available: http://www.iccm-central.org/Proceedings/ICCM17proceedings/Themes/Behaviour/FAILURE%20CRITERIA%20FOR%20DES/F12.3%20Sanford.pdf. [Accessed 16 October 2016].

[4] Simulia, "Abaqus Analysis User's Guide," [Online]. [Accessed 2016 August 2016].

[5] C. Sun, Mechanics of Composite Materials and Laminates, West Lafayette: Purdue University, 2001.

[6] R. Talreja, "Assessment of the Fundamentals of Failure Theories for Composite Materials," *ELSEVIER,* 2015.

[7] M. Hinton, A. S. Kaddour and P. D. Soden, Failure Criteria in Fibre Reinforced Polymer Composites: The World-Wide Failure Exercise, San Diego: ELSEVIER, 2004.

[8] G. Alfano and M. A. Crisfield, "Finite Element Interface Models for the Delamination Analysis of Laminated Composites: Mechanical and Computational Issues," *International Journal for Numerical Methods in Engineering,* 2001.

[9] G. Ramakrishna, "Delamination of C/PEEK I-Beam Using Virtual Crack Closure Technique and Cohesive Zone Method," Purdue University, West Lafayette, 2015.

[10] Z. Hashin, "Failure Criteria for Unidirectional Fiber Composites," *Journal of Applied Mechanics,* vol. 47, pp. 329-334, 1980.

[11] E. F. Rybicki and M. F. Kanninen, "A Finite Element Calculation of Stress Intensity Factor by a Modified Crack Closure Integral," *Engineering Fracture Mechanics,* vol. 9, pp. 931-938, 1977.

[12] G. Irwin, "Analysis of Stresses and Strains Near the End of a Crack Transversing a Plate," *Journal of Applied Mechanics,* vol. 24, pp. 361-366, 1957.

[13] I. Raju, "Calculation of Strain-Energy Release Rates with Higher Order and Singular Finite Elements," *Engineering Fracture Mechanics,* vol. 28, pp. 251-274, 1987.

[14] O. Allix, P. Ladeveze and A. Corigliano, "Damage Analysis of Interlaminar Fracture Specimens," *Composite Structures,* vol. 31, pp. 66-74, 1995.

[15] O. Allix and A. Corigliano , "Modeling and Simulation of Crack Propagation in Mixed-Modes Interlaminar Fracture Specimens," *International Journal of Fracture,* vol. 77, pp. 111-140, 1996.

[16] N. Point and E. Sacco, "A Delamination Model for Laminated Composites," *International Journal of Solids and Structures,* vol. 33, pp. 483-509, 1996.

[17] J. Schellekens and R. De Borst, "A Non-linear Finite Element Approach for the Analysis of Mode I Free Edge Delamination in Composites," *International Journal of Solids and Structures,* vol. 30, pp. 1239-1253, 1993.

[18] D. Bruno and A. Grimaldi, "Delamination Failure of Layered Composite Plates Loaded in Compression," *International Journal of Solids and Structures,* vol. 20, pp. 3-11, 1990.

[19] J. Chaboche, R. Girard and A. Schaff, "Numerical Analysis of Composite Systems by using Interphase/Interface Models," *Computational Mechanics,* vol. 20, pp. 3-11, 1997.

[20] A. Corigliano, "Formulation, Identification and Use of Interface Models in the Numerical Analysis of Composite Delamination," *International Journal of Solids and Structures,* vol. 30, pp. 2779-2811, 1993.

[21] G. Bolzon and A. Corigliano, "A Discrete Formulation for Elastic Solids with Damaging Interfaces," *International Journal of Solids and Structures,* vol. 140, pp. 329-359, 1997.

[22] Y. Mi, M. Crisfield, H. Hellweg and G. Davies, "Finite Element Method and Progressive Failure Modelling of Composite Structures," in *Computational Plasticity: Fundamentals and Applications*, Barcelona, 1997, pp. 239-254.

[23] J. Chen , M. Crisfield, A. Kinloch, F. Matthews, E. Busso and Y. Qiu, "The Application of Interface Elements in Predicting Progressive Delamination of Composite Material Specimens," in *Proceedings of the Conference: Mechanics of Composite Materials and Structures*, Portugal, 1998.

[24] Y. Mi, M. Crisfield, G. Davies and H. Hellweg, "Progressive Delamination Using Interface Elements," *Journal of Composite Materials,* vol. 32, pp. 1246-1272, 1998.

[25] A. Hilleborg, M. Modeer and P. Peterson, "Analysis of Crack Formation and Growth in Concrete by Means of Fracture Mechanics and Finite Elements," *Cement and Concrete Research,* vol. 6, pp. 773-782, 1976.

[26] V. Tvergaard and J. Hutchinson, "The Influence of Plasticity on Mixed-Mode Interface Toughness," *Journal of the Mechanics and Physics of Solids,* vol. 41, pp. 1119-1135, 1993.

[27] S. P. Engelstad and S. B. Clay, "Comparison of Composite Damage Growth Tools for Static Behavior of Notched Composite Laminates," *Journal of Composite Materials,* 2016.

[28] A. Griffith, "The Phenomena of Rupture and Flow in Solids," *Philosophical Transactions of the Royal Society, London,* vol. 221, no. Series A, pp. 163-198, 1921.

[29] P. Robinson, T. Besant and D. Hitchings, "Delamination Growth Prediction Using A Finite Element Approach," in *2nd ESIS TC4 Conference on Polymers and Composites*, Les Diablerets, Switzerland, 1999.

[30] Y. Wei and J. W. Hutchinson, "Interface Strength, Work of Adhesion and Plasticity in the Peel Test," *International Journal of Fracture,* vol. 93, pp. 315-333, 1998.